UNIVERSIDADE DE SÃO PAULO

FACULDADE DE FILOSOFIA, CIÊNCIAS E LETRAS DE RIBEIRÃO PRETO

PROGRAMA DE PÓS-GRADUAÇÃO EM FÍSICA APLICADA À MEDICINA E BIOLOGIA

GABRIELA PAZIN TARDELLI

Blindagem de Ferrita para melhorar a performance de Magnetômetros de bombeamento óptico para Magnetocardiografia fetal

Ferrite shield to enhance the performance of Optically Pumped Magnetometers for Fetal Magnetocardiography

Ribeirão Preto – SP

2023

UNIVERSIDADE DE SÃO PAULO

FACULDADE DE FILOSOFIA, CIÊNCIAS E LETRAS DE RIBEIRÃO PRETO

PROGRAMA DE PÓS-GRADUAÇÃO EM FÍSICA APLICADA À MEDICINA E BIOLOGIA

Blindagem de Ferrita para melhorar a performance de Magnetômetros de bombeamento óptico para Magnetocardiografia fetal

Ferrite shield to enhance the performance of Optically Pumped Magnetometers for Fetal Magnetocardiography

GABRIELA PAZIN TARDELLI

Versão Corrigida

Dissertação apresentada à Faculdade de Filosofia, Ciências e Letras de Ribeirão Preto da Universidade de São Paulo, como parte das exigências para a obtenção do título de Mestre em Ciências.

Área de concentração: Física Aplicada à Medicina e Biologia.

Orientador: Prof. Dr. Oswaldo Baffa Filho

Coorientador: Prof. Dr. Ronald T. Wakai

Ribeirão Preto – SP

2023

Catalogação da Publicação

Serviço de Documentação da Universidade de São Paulo

Faculdade de Filosofia, Ciências e Letras de Ribeirão Preto

Tardelli, Gabriela Pazin

Ferrite shield to enhance the performance of Optically Pumped Magnetometers for Fetal Magnetocardiography / Gabriela Pazin Tardelli; orientador Oswaldo Baffa Filho, coorientador Ronald Wakai. Ribeirão Preto – SR, 2023.

59 f.: il.

Dissertação (Mestre em Ciências) – Programa de Pós-Graduação em Física Aplicada à Medicina e Biologia, Faculdade de Filosofia, Ciências e Letras de Ribeirão Preto, Universidade de São Paulo, 2023.

Orientador: Prof. Dr. Oswaldo Baffa Filho

Coorientador: Prof. Dr. Ronald T. Wakai

1. Blindagem magnética. 2. Ferrita. 3. Magnetocardiografia fetal. 4. Magnetômetros de bombeamento óptico. 5. Arritmias fetais.

Nome: TARDELLI, Gabriela Pazin

Título: Ferrite shield to enhance the performance of Optically Pumped Magnetometers for Fetal Magnetocardiography

Dissertação apresentada à Faculdade de Filosofia, Ciências e Letras de Ribeirão Preto para obtenção do título de Mestre em Ciências.

Aprovado em: 27 de abril de 2023

Banca Examinadora

Prof. Dr. Oswaldo Baffa Filho

Professor Titular no Departamento de Física da Faculdade de Filosofia, Ciências e Letras de Ribeirão Preto da Universidade de São Paulo

Julgamento: Aprovado

Prof. Dr. José Ricardo de Arruda Miranda

Professor Titular no Departamento de Biofísica e Farmacologia do Instituto de Biociências da UNESP

Julgamento: Aprovado

Prof. Dra. Elizabeth Costa Monteiro

Professora no Departamento de Metrologia da Pontifícia Universidade Católica do Rio de Janeiro

Julgamento: Aprovado

Ao meu pai Paulo, minha mãe Rosemir e meus irmãos Lidieli e Gustavo!

ACKNOWLEDGMENTS

Gostaria de expressar os meus sinceros agradecimentos a todos aqueles que contribuíram para a conclusão desta dissertação.

Em primeiro lugar, meu profundo agradecimento aos meus coorientadores, Professor Oswaldo Baffa e Professor Ronald Wakai. Primeiramente, ao Professor Baffa que ao longo de 6 anos - incluindo minha iniciação científica e mestrado - foi meu grande mentor. Obrigada por seu apoio e orientação inestimável ao longo desta jornada. Sou muito grata pelo privilégio de poder aprender e trabalhar ao seu lado. Tenho enorme admiração não apenas pelo seu trabalho incrível como cientista, mas também pela sua forma de viver a vida, sempre muito alegre e bondoso. Ao Professor Wakai, agradeço a oportunidade incrível de fazer parte de seu laboratório e trabalhar ao seu lado. Foi um grande privilégio aprender com alguém tão dedicado e experiente como o senhor. Agradeço também por me receber tão bem em Madison, sempre muito gentil e atencioso, e por todo o suporte profissional e pessoal na minha adaptação. O conhecimento me passado por vocês é um grande molde à profissional que sou hoje. Eterna gratidão!

Também sou grata aos meus colegas de laboratório da USP, Petrus, Thais, Leonardo, e em especial Victor e Renan. Muito obrigada pelos anos de amizade, companheirismo, conversas de laboratório, desabafos pessoais, e incontáveis cafés. Agradeço também ao Tan, meu colega na UW-Madison, pelo acolhimento, paciência, amizade, e inúmeras dicas de inglês. Aos funcionários da secretaria, Nilza e Denise, pela paciência e compreensão durante todo o processo burocrático, e aos técnicos Carlos Renato, Lourenço e Fernando pelo trabalho impecável com a blindagem instalada na USP.

Agradeço a todos os amigos que conquistei ao longo destes anos. Em especial as minhas amizades de Ribeirão Preto: Siqueira, Recruta, Popeye e Lilo. E aos meus amigos de Madison: Tati, Nikola, Iago, Lucas e Michele. Obrigada por todo apoio, incentivo e risadas que vivemos juntos. Às três repúblicas especiais que fizeram parte da minha trajetória e na qual construí grandes amizades: Rep VaiDáNada, Rep ViraTudo e Rep Gruta. Vocês foram muito importantes no meu crescimento e tenho um carinho especial por cada um.

Além disso, gostaria de estender minha gratidão à minha família. Aos meus pais, Paulo e Rosemir, que me deram muito suporte desde o início da minha educação até minha busca pela

carreira acadêmica. Que me apoiaram durante todo meu processo de mudança para o exterior, ouviram pacientemente meus anseios e ofereceram sabedoria e amor em todas as situações. Suas crenças inabaláveis e encorajamento me impulsionaram a ser a mulher que sou hoje. Aos meus irmãos, Lidieli e Gustavo, pela amizade e companheirismo que compartilhamos um ao outro, e por estarem sempre ao meu lado e dispostos a me ouvir e ajudar. Á Raisa que ao longo dos anos se tornou minha irmã de coração e esteve presente nos momentos mais importantes da minha vida. À minha família do coração, Bruno, Nayara e Alice que foram meu grande suporte durante a pandemia.

Gostaria de agradecer aos participantes deste estudo, cuja generosidade e disposição em compartilhar seu tempo e experiências tornaram esta pesquisa possível. Sem a sua inestimável contribuição, esta dissertação não teria sido possível.

E agradeço aos membros da banca por aceitarem o convite e contribuírem para conclusão deste mestrado.

Obrigado a todos por suas contribuições, apoio e incentivo. Esta dissertação não teria sido possível sem vocês. Muito obrigada!

Este trabalho recebeu financiamento do Conselho Nacional de Desenvolvimento Científico e Tecnológico (CNPq; 30439/2021-5), da Fundação de Amparo à Pesquisa do Estado de São Paulo (FAPESP; 2021/06224-4), e da Universidade de Wisconsin-Madison através do National Institutes of Health (R01 HL63174; R01 HL 345 143485).

RESUMO

TARDELLI, G. P. **Blindagem de Ferrita para melhorar a performance de Magnetômetros de bombeamento óptico para Magnetocardiografia fetal.** 2023. Dissertação (Mestrado em Física Aplicada a Medicina e Biologia) – Faculdade de Filosofia, Ciências e Letras de Ribeirão Preto, Universidade de São Paulo, Ribeirão Preto - SP, 2023).

Magnetocardiografia fetal (fMCG) é uma técnica não invasiva para monitoramento da atividade elétrica cardíaca durante a gravidez. FMCG fornece informações relevantes sobre a eletrofisiologia cardíaca de fetos, melhorando o diagnóstico e prognóstico de arritmias fetais. Similar à eletrocardiografia fetal (fECG), que registra o campo elétrico produzido pela corrente elétrica do coração fetal, a fMCG mede o campo magnético produzido pela mesma corrente. Embora a fECG já esteja disponível há algum tempo, a baixa resolução do sinal limitou seu uso clínico. Em contraste, a fMCG apresenta vantagens sobre outras ferramentas de monitoramento cardíaco fetal, porém sua adoção foi limitada pelo alto custo dos Dispositivos Supercondutores de Interferência Quântica (SQUID). Avanços recentes em física atômica e tecnologia quântica levaram ao desenvolvimento de magnetômetros de bombeamento óptico (OPMs), que podem atingir a mesma sensibilidade a um custo e tamanho reduzido, e sem a necessidade de criogenia. Além disso, OPMs podem ser operados dentro de blindagens cilíndricas do tamanho de uma pessoa, tornando a fMCG mais prática. No entanto, para garantir o conforto do paciente e evitar claustrofobia, uma das extremidades da blindagem é mantida aberta. Por consequência, a interferência magnética ambiental entra pela abertura da blindagem e degrada a qualidade dos sinais de fMCG, especialmente na direção longitudinal. Este estudo teve como objetivo atenuar essas interferências colocando a matriz de OPMs dentro de uma pequena blindagem de ferrita. Embora o sinal fetal tenha sido ligeiramente atenuado, a interferência ambiental foi reduzida substancialmente, assim como a interferência materna. Isso aumentou significativamente a relação sinal-ruído e melhorou a resolução de pequenas componentes da forma de onda. A blindagem de ferrita conferiu uma vantagem significativa ao permitir a medição da componente longitudinal do sinal fMCG, que anteriormente era fortemente afetado pela interferência ambiental, com eficiência comparável as outras componentes. A blindagem de ferrita resultou em uma caracterização mais abrangente do sinal de fMCG e, portanto, oferece uma alternativa prática e econômica para aprimorar o sistema OPM-fMCG.

Palavras chave: 1. Blindagem magnética. 2. Ferrita. 3. Magnetocardiografia fetal. 4. Magnetômetros de Bombeamento Óptico. 5. Arritmias fetais

ABSTRACT

TARDELLI, G. P. **Ferrite shield to enhance the performance of Optically Pumped Magnetometers for Fetal Magnetocardiography.** 2023. Dissertation (M.Sc. in Physics Applied to Medicine and Biology) – School of Philosophy, Sciences, and Letters of Ribeirão Preto, University of São Paulo, Ribeirão Preto - SP, 2023).

Fetal magnetocardiography (fMCG) is a non-invasive technique for monitoring electrical cardiac activity during pregnancy. FMCG provides valuable information about fetal cardiac electrophysiology, improving the diagnosis and prognosis of fetal arrhythmias. Similarly, to fetal electrocardiography (fECG), which records the electric field produced by the electrical current flowing through the fetal heart, fMCG measures the magnetic field produced by the same current. Although fECG has been available for some time, its poor signal resolution has limited its use in clinical practice. In contrast, fMCG has advantages over other fetal cardiac monitoring tools, but its adoption has been limited by the high cost of Superconducting Quantum Interference Devices (SQUID). Fortunately, recent advances in atomic physics and quantum technology have led to the development of Optically Pumped Magnetometers (OPMs), which can achieve the same sensitivity at a lower cost, without the need for cryogenics, and with a smaller size. In addition, OPMs can operate within person-sized cylindrical shields, making fMCG more practical. However, one end of the shield is kept open to ensure patient comfort and prevent claustrophobia. Consequently, environmental magnetic interference can enter through the shield opening and degrade the quality of fMCG signals, especially in the longitudinal direction. This study aimed to attenuate these interferences by placing the OPM array within a small ferrite shield. Although the fetal signal was slightly attenuated, the environmental interference was reduced substantially, as well as the maternal interference. This increased the signal-to-noise ratio significantly and improved the resolution of the smaller cardiac waveform components. The ferrite shield conferred a significant advantage by enabling the measurement of the longitudinal component of the fMCG signal, which had previously been overwhelmingly affected by environmental interference, with comparable efficiency as the other components. The ferrite shield resulted in a more comprehensive characterization of the fMCG signal and, therefore, offers a practical and cost-effective alternative to enhance the OPM-fMCG system.

Keywords: 1. Magnetic shielding. 2. Ferrite. 3. Fetal magnetocardiography. 4. Optically Pumped Magnetometers. 5. Fetal arrhythmias.

LIST OF FIGURES

LIST OF TABLES

LIST OF ABBREVIATIONS

ANOVA	Analysis of Variance
AV	Atrioventricular
bpm	Beats per minute
fECG	Fetal electrocardiography
fQRS	Fetal QRS complex
FHR	Fetal heart rate
fMCG	Fetal magnetocardiography
ICA	Independent Component Analysis
LQTS	Long QT Syndrome
mQRS	Maternal QRS complex
MEG	Magnetoencephalography
MSR	Magnetically shielded room
OPM	Optically Pumped Magnetometer
PAC	Premature atrial contraction
PVC	Premature ventricular contraction
SA	Sinoatrial
SNR	Signal-to-noise ratio
SQUID	Superconducting Quantum Interference Device
T	Tesla
TdP	Torsades de Points

SUMMARY

1. GENERAL CONCEPTS

This section provides a review of the concepts essential to this research. It covers the anatomy, function, and electrophysiology of the heart, focusing on fetal arrhythmias. Different fetal heart monitoring modalities are compared, emphasizing fetal magnetocardiography (fMCG). The gold standard magnetic sensor – Superconducting Quantum Interference Device (SQUID) – and an innovative alternative, Optically Pumped Magnetometers (OPMs), are described. Lastly, concepts involving magnetic shields and their importance for maintaining a low background magnetic field to enable weak signal recording like fMCG are explored.

1.1. Heart and Electrical Conduction

The heart is one of the most vital organs of the human body. It has the main function of receiving blood full of carbon dioxide and waste products from the body to be eliminated by the lungs, and pumping blood full of oxygen and nutrients to the body. The heart works continuously to ensure that all the body's tissues receive the oxygen and nutrients they need to function properly.

The heart is divided into four chambers – two upper chambers (right and left atrium) and two lower chambers (right and left ventricles). The vessels – arteries, capillaries, and veins – carry the blood through the chambers, and the valves act like gates between the chambers, keeping the blood flowing in the forward direction. The right atrium receives oxygen-poor blood from the body through the superior and inferior vena cava and pumps it to the right ventricle through the tricuspid valve. The right ventricle pumps this blood to the lungs through the pulmonary artery. The lungs remove the carbon dioxide from the blood through diffusion, reload it with oxygen, and send oxygen-rich blood to the left atrium through the pulmonary vein. The left atrium pumps the blood to the left ventricle through the mitral valve, which pumps it back to the rest of the body through the aorta, as depicted in Figure 1 (BETTS et al., 2017; HALL; GUYTON, 2017)

Figure 1 Structure of the heart and course of blood flow through the heart chamber and valves.

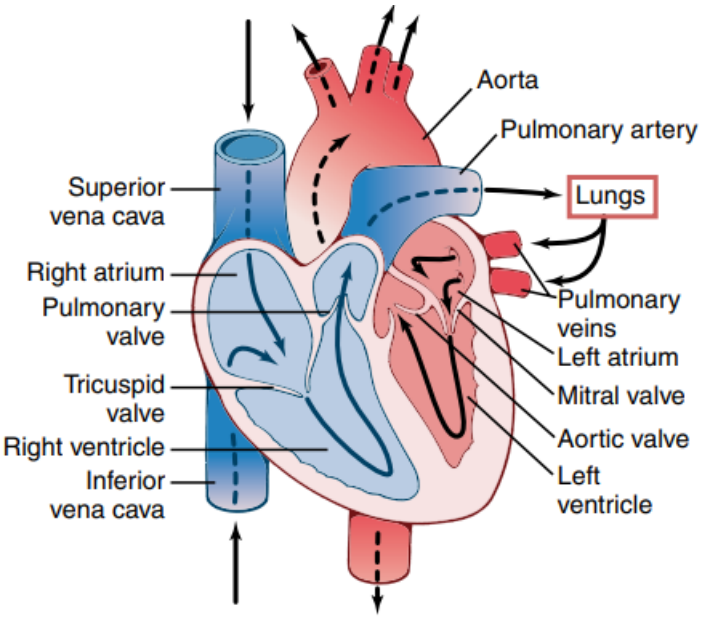

Reproduced from (HALL; GUYTON, 2017)

To pump blood through the heart, the cardiac muscle has to contract and relax. The timing and coordination of the heart's contractions are controlled by electrical signals. The heart has a small number of conducting cells that spread the electrical signal throughout the heart and a higher number of contractile cells responsible for heart contraction. Pacemaker cells in the sinoatrial (SA) node spontaneously depolarize, generating an action potential, which is a variation of the membrane potential due to the inflow and outflow of ions. This electrical impulse propagates through the conducting cells throughout the conduction system, which triggers the contractile cells to make the cardiac muscle contract (BETTS et al., 2017).

The cardiac conduction system starts in the SA node, located in the right atrium near the superior vena cava. The self-excitatory cells of the SA node generate the action potentials at a regular rate, causing the contraction of the atrial muscles. The electrical signal flows to the atrioventricular (AV) node located at the boundary between the atria and ventricle. Then, the two branches of the bundle of His carry the electrical signal from the AV node to the Purkinje fibers, which diverge into the ventricular wall causing them to depolarize and contract (BETTS et al., 2017).

The graphic representation of the heart's electrical activity over time is the electrocardiogram tracing (BETTS et al., 2017; HALL; GUYTON, 2017; HIRSH; SOUTHMAYD, 2020), which is observed in Figures 2 and 3. The depolarization of the atria is represented by the P-wave (Figure 2 (2)). The time interval from the arrival of the electrical impulse in the AV node and its propagation throughout the Bundle of His and Purkinje fibers

is represented by the PR interval (Figure 2 (3)). The repolarization of the atria is not graphically present because it occurs at the same time the ventricles depolarize. The depolarization/contraction of the ventricles is the QRS complex (Figure 2 (4)), and the repolarization is the T-wave (Figure 2 (6)); therefore, the QT interval represents the time it takes for the ventricles to contract and repolarize. A small U-wave is seen in some people and represents the repolarization of the Purkinje fibers. The time interval between two consecutive R-waves (RR interval) is used to calculate the heart rate, which indicates the number of times the heart beats per minute (bpm).

Figure 2 Diagram of each event of the heart's electrical and mechanical activity and its respective representation in the electrocardiogram tracings.

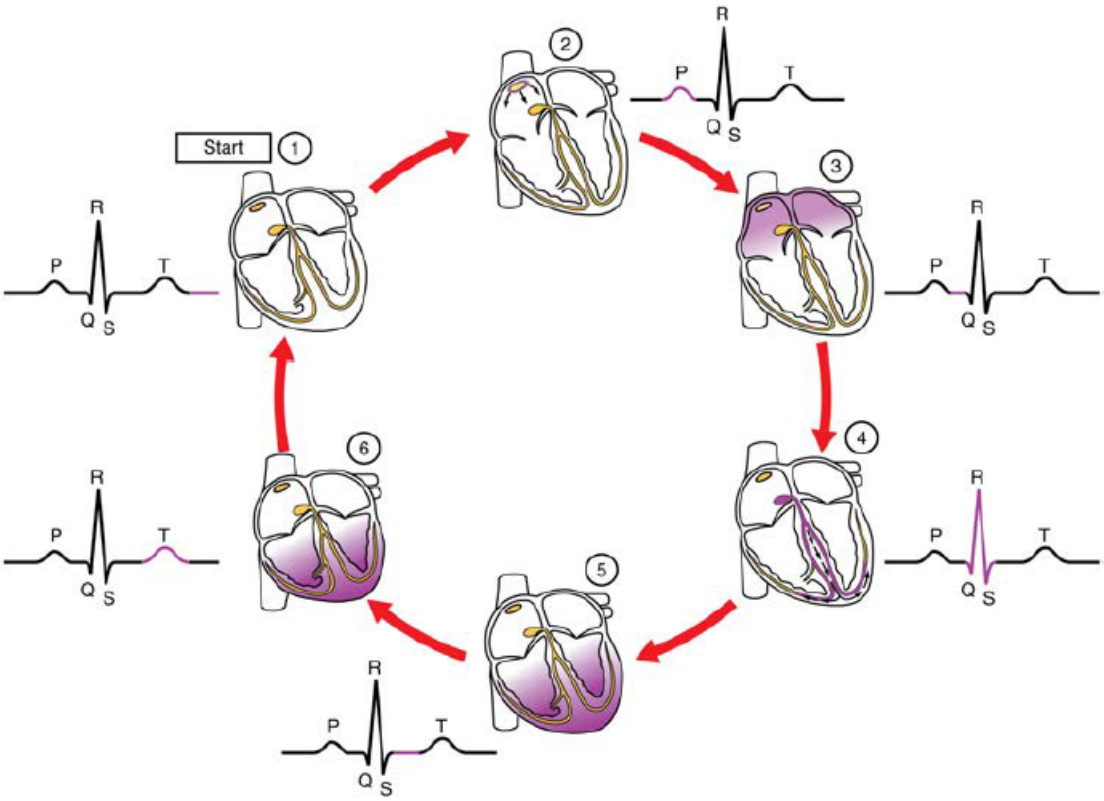

Reproduced from (BETTS et al., 2017)

Figure 3 Cardiac waveform and its intervals

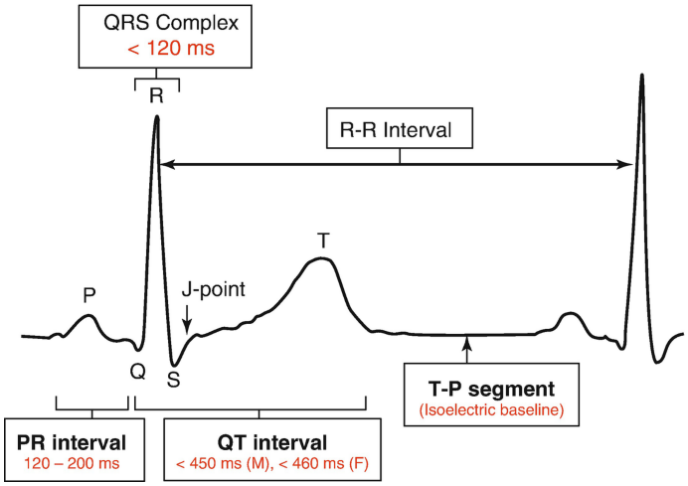

Reproduced from (HIRSH; SOUTHMAYD, 2020)

1.2. Fetal Heart and Arrhythmias

The heart is the first organ to develop during organogenesis (BETTS et al., 2017). On the 18th day of life, a primitive blood vessel starts to form in a cardiogenic area near the head of the embryo. From the 20th to the 28th day, this primitive vessel changes into recognizable structures similar to an adult heart. By the end of the 8th week, the atria and ventricles are partitioned into four chambers. The fetal heart is similar to that of an adult, except for two features – foramen ovale and ductus arteriosus – that shunt blood away from the pulmonary circulation as the lungs don't function and the exchange of nutrients occurs through the placenta (ADLER; FREEBORN; TREVINO). Despite this anatomical difference, the electrical conduction system is very similar. The phases of the fetal heart development are depicted in Figure 4.

Figure 4 Embryological development of the human heart from the beginning of the cardiogenesis to the formation of four chambers.

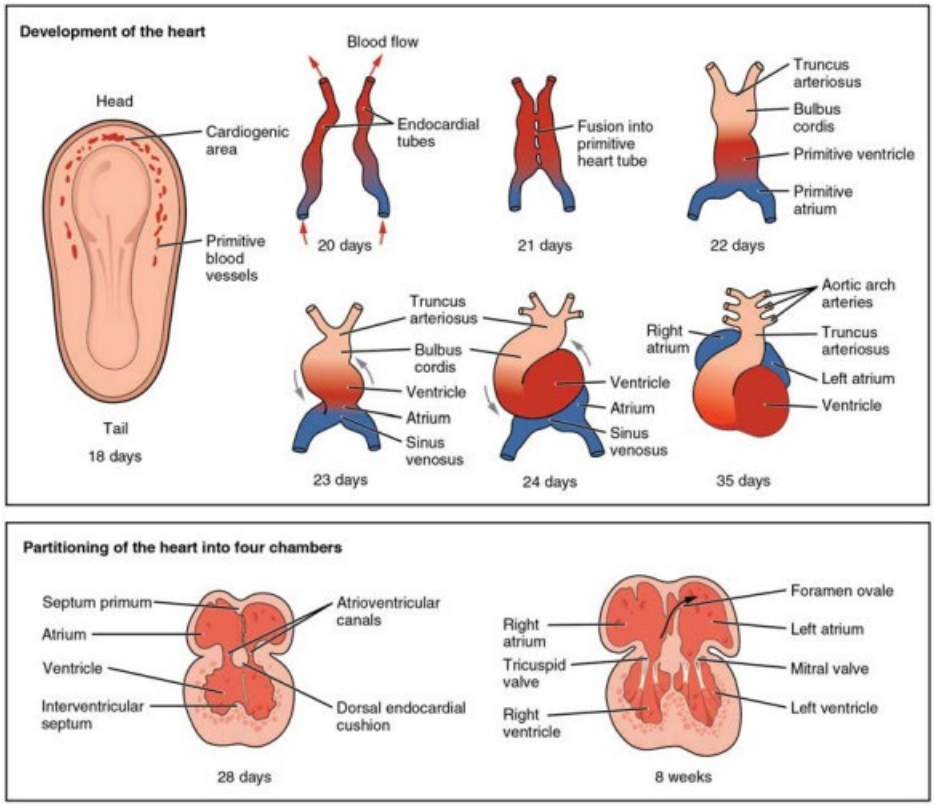

Reproduced from (BETTS et al., 2017)

The fetal heart begins to beat around 6 weeks of gestational age at a rate of approximately 110 bpm. At 9-10 weeks, the fetal heart rate (FHR) is about 170 bpm. At 14 weeks, it gradually decreases to 150 bpm until it reaches 130 bpm at 40 weeks of gestational age. The FHR of a normal fetus ranges from 110-180 bpm (HORNBERGER; SAHN, 2007; HYETT et al., 1996; LIAO et al., 2000; REMPEN, 1990; ROBINSON; SHAW-DUNN, 1973). The FHR is faster than an adult's, which ranges from 60-100 bpm. Some differences are also observed between the fetal and adult electrical waveforms. The QRS complex of fetuses is narrower, and the T-wave is typically flatter. These differences are normal and reflect the developmental changes in the heart from fetal to adult life. However, differences in the morphology, interval duration, and/or FHR out of the normal range might indicate abnormal conduction of the electrical activity in the heart, which means a possible heart condition.

In fetuses, arrhythmias are relatively rare but can have severe consequences for fetal development and survival. An FHR higher than 180 bpm is considered tachycardia and can be classified into sinus tachycardia, supraventricular tachycardia, atrial tachycardia, and atrial flutter. In contrast, an FHR lower than 110 bpm is considered bradycardia and might indicate sinus bradycardia, blocked atrial ectopy, AV block, or long QT syndrome (LQTS). Ectopy is a

third type of arrhythmia that presents with extra beats (MATTA; CUNEO, 2010; STRASBURGER; CHEULKAR; WICHMAN, 2007) and is usually benign, although it can be associated with other heart defects (CUNEO et al., 2006; SIMPSON; YATES; SHARLAND, 1996). Ectopy can be separated into premature atrial contractions (PACs) if it originates in the atria, and premature ventricular contractions (PVCs) if originates in the ventricles. Moreover, other fetal cardiac conditions can be assessed by changes in the waveform morphology, polarity, and interval duration. For instance, a prolonged QT interval is a potential sign of LQTS, which can cause Torsades de Points (TdP), a severe arrhythmia associated with syncope, seizures, and sudden death (CUNEO; STRASBURGER; WAKAI, 2016). Diagnosing LQTS before birth can aid in managing prenatal medication that minimizes the chances of TdP in the fetus, thus preventing intrauterine fetal demise (CROTTI et al., 2013) or Sudden Infant Death Syndrome (SCHWARTZ, 2004).

1.3. Fetal Heart Monitoring Modalities

Some fetal arrhythmias can be serious and may require treatment in utero or immediately after delivery. Assessing fetal cardiac electrical activity can help diagnose fetal arrhythmias and guide management. Here, we describe three non-invasive diagnostic modalities of prenatal fetal cardiac monitoring.

1.3.1. Fetal Echocardiography

Fetal echocardiography is the most widely used technique for fetal surveillance. It is non-invasive, practical, and affordable. It can be performed as early as 6 weeks of gestational age, although it is usually performed after 18 weeks in healthy fetuses or 14 weeks if there is any factor of risk. Fetal echocardiography uses an ultrasound device to obtain the mechanical activity of the fetus' heart. This technique is versatile because it can operate in various modes, with M-mode and Pulsed Doppler being the most common for evaluating fetal arrhythmias.

Fetal echocardiography can provide detailed information about the structure and function of the fetal heart, including blood flow patterns, valve function, and any structural abnormalities. The heart's electrical activity, however, is not directly measured by fetal echocardiography. Instead, mechanical events such as atrial and ventricular contractions are used to infer these electrophysiological events. In other words, the abnormal fetal rhythm is assessed by the mechanical consequence of the arrhythmia instead of the conduction itself (STRASBURGER; WAKAI, 2010). The diagnosis is limited to the atrioventricular relationship and the atrial and ventricular rate (HORNBERGER, 2007). However, certain repolarization

abnormalities, such as QTc prolongation or ST segment changes, require knowledge of the heart's electrical conduction to be accurately diagnosed. Furthermore, certain arrhythmias can occur intermittently, underscoring the importance of monitoring the heart over longer periods to ensure that the arrhythmia will be detected. Using ultrasound can be challenging due to fetal movement and positioning, as well as the physician's ability to maintain the probe stable over extended periods. Despite this limitation, fetal echocardiography plays an important role in fetal cardiac management.

1.3.2. Fetal Electrocardiography

Fetal electrocardiography (fECG) measures the electric field produced by the electrical current propagating through the conduction system of the fetus' heart (CLIFFORD et al., 2014). fECG is more practical, less expensive, and can directly measure the electrical activity of the fetus' heart as early as 17 weeks of gestational age (TAYLOR et al., 2003). fECG has the advantage of enabling long-term recordings in the home environment (MARIA et al., 1995; PIERI et al., 2001), facilitating the identification of intermittent arrhythmias. The drawback of ECG is the poor signal resolution due to the electrode being in contact with the mother's abdomen rather than directly with the fetus. As a result, small components such as P- and T-wave morphology are not always interpretable. In addition, from the 28th to 34th week of pregnancy, fECG signals are attenuated by amniotic fluid and the *vernix caseosa*, a protective substance that covers the fetus and acts as an electrical insulator (OLDENBURG; MACKLIN, 1977; WAKAI; LENGLE; LEUTHOLD, 2000). Although the ECG is the primary diagnostic modality for adult cardiac rhythm assessment, it is not routinely used for screening purposes in fetuses. Instead, fECG is mainly limited to monitoring during labor.

1.3.3. Fetal Magnetocardiography

fMCG is a precise, accurate, and direct technique for assessing fetal electrical cardiac activity. It is the magnetic analog of fECG as it measures the magnetic fields generated by the same electrical activity of the fetal heart and shows the same features – P-wave, QRS complex, and T-wave (PETERS; STINSTRA; UZUNBAJAKAU, 2005).

Unlike fECG, the fMCG signal does not suffer attenuation from the *vernix caseosa*; thus, it can be recorded from the 20th of pregnancy onward (WAKAI; LENGLE; LEUTHOLD, 2000). However, the magnetic field generated by the fetal heart is low in amplitude. Specifically, the QRS complex, the most prominent component, typically has an amplitude on the order of 1 pT during the 20-30' week gestational period (LABYT; SANDER; WAKAI,

2022). As the gestational age progresses, the signal amplitude increases (STRAND; STRASBURGER; WAKAI, 2019). To accurately measure such a weak signal, ultrasensitive devices and a highly magnetically shielded environment are necessary. Additionally, optimizing the distance between the heart and sensor is crucial, as the signal quality deteriorates with the distance.

FMCG provides valuable electrophysiological and behavioral information, including rhythm, waveform morphology, cardiac time intervals, FHR variability, and fetal activity (KHLER et al., 2002; LEEUWEN et al., 1999; STINSTRA et al., 2002; STRASBURGER; WAKAI, 2010; WAKAI, 2004; ZHAO et al., 2002). FHR reactivity, i.e., FHR acceleration in association with fetal movement, is an important indicator of fetal well-being (ZIZZO et al., 2020). Fetal arrhythmias and congenital heart diseases were investigated with fMCG in several studies (CUNEO et al., 2013; KÄHLER et al., 2002; WACKER-GUSSMANN et al., 2014, 2016; WACKER-GUSSMANN; STRASBURGER; WAKAI, 2022; WAKAI et al., 2003; WIGGINS et al., 2013; ZHAO et al., 2006, 2008). The use of fMCG for diagnoses of fetal arrhythmias was endorsed by the American Heart Association in its inaugural Statement on Diagnosis and Treatment of Fetal Cardiac Disease (DONOFRIO et al., 2014). Therefore, fMCG has emerged as a complementary diagnostic tool to fetal echocardiography and an alternative to fetal electrocardiography.

1.4. Sensors

The magnetic fields generated from the fetus' heart activity are very weak (on the order of 10^{-11} T); thus, magnetic sensors with the highest possible sensitivity are needed. For 30 years, SQUIDs were the only magnetometers with sufficient sensitivity to record fMCG signals. Recent advances in atomic physics and quantum technology have led to the development of the OPM that can also achieve the required sensitivity.

1.4.1. Superconducting Quantum Interference Device

The SQUID was used for the first time for biomedical purposes in 1970 (COHEN; EDELSACK; ZIMMERMAN, 1970). The first measurement was an adult magnetocardiogram, and since then, its application to other biomedical measurements has grown rapidly, including the measurement of the fMCG in 1974 (KARINIEMI et al., 1974). Currently, the SQUID is the only device with Food and Drug Administration approval for fetal cardiac assessment.

A SQUID consists of a superconducting loop interrupted by two Josephson junctions. A Josephson junction is a tunneling barrier between two superconducting materials, which allows a flow of supercurrent (a current carried by pairs of electrons) between them. When a magnetic field is applied to the SQUID, it induces a small circulating current in the superconducting loop, which generates a magnetic flux. This flux causes a change in the critical current of the Josephson junctions, which alters the phase difference between the supercurrents flowing through them. This change in phase difference results in a change in voltage across the SQUID. Small changes in the magnetic field can produce large changes in the voltage output as the SQUID's response to the magnetic field is nonlinear (FAGALY, 2006).

The SQUID, illustrated in Figure 5, was the most sensitive magnetic sensor available for a long time. It can measure magnetic fields on the order of femtotesla (fT); therefore, it can easily detect low biomagnetic signals, such as fetal cardiac signals. Additionally, SQUIDs have the great advantage of working as gradiometers. A gradiometer consists of two identical and parallel coils separated by a certain distance, with one coil measuring both the environmental and source magnetic field and the other measuring the environmental field. The difference between the two measurements provides the magnetic field of the source alone. Gradiometers are useful for detecting weak sources of magnetic fields near the detection device. They can measure changes in the field without being affected by a strong uniform field originating from farther away (FAGALY, 2006)

The state of superconductivity required for the SQUIDs to operate only occurs at very low temperatures, typically less than 10 K (-263 °C), which is achieved through cryogenic cooling. However, cryogenic cooling demands large amounts of liquid helium, resulting in weekly investments to maintain the system's functionality. Additionally, due to the large size of the Dewar used to store the liquid helium, an entire magnetically shielded room (MSR) is necessary to ensure a low magnetic field environment. The whole system can cost up to a million dollars, with additional expenses for liquid helium. Consequently, the investment required to implement SQUIDs is not easily recoverable for hospitals and clinics through billings. Despite its great sensitivity in evaluating biomagnetic signals, SQUID-based systems have been limited to only a few research centers due to the high cost.

Figure 5 Design of SQUID components (Dewar, sensors, detection coils) in an adult MCG measurement.

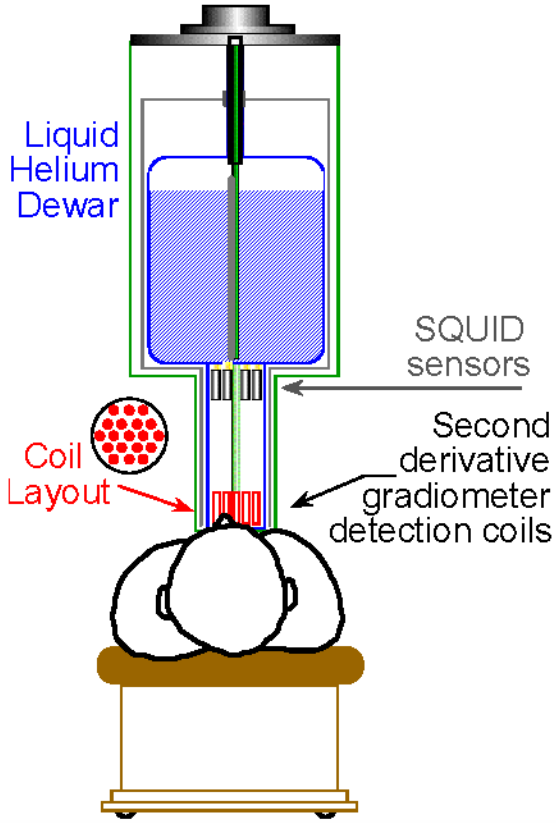

Reproduced from (FAGALY, 2006)

1.4.2. Optically Pumped Magnetometer

OPMs – or atomic magnetometers – were first developed in the 1950s (BELL; BLOOM, 1957; DEHMELT, 1957). Over the years, several groups have contributed to making the OPMs smaller, less complex, and more sensitive (DUPONT-ROC; HAROCHE; COHEN-TANNOUDJI, 1969; HAPPER; TANG, 1973; KOMINIS et al., 2003; SHAH et al., 2007; SHAH; WAKAI, 2013). The major advantage is the elimination of cryogenic cooling requirements. This makes OPMs a one-time investment that doesn't require ongoing expenses to keep them functioning. For low channel-count applications like fMCG, an OPM system with the same number of channels as a SQUID system can be approximately ten times less expensive. Currently, a few commercial versions of OPMs are available on the market. However, as it is a technology in development, OPM is still limited as an investigational device for research involving fetal cardiac assessment.

The OPM consists of a diode laser to generate resonant light, a transparent glass alkali vapor cell, and a photodetector (TIERNEY et al., 2019). The resonant light spin-polarizes the atoms in the gas. In a quasi-zero magnetic field environment, if a second laser beam is applied

to the cell, it will pass through the vapor cell and reach the photodetector with maximum intensity. In the presence of a magnetic field, however, the net polarization will rotate by a slight angle. Then, the light from the laser beam will be partially absorbed by the atoms, and a change in the transmitted light intensity is measured by a photodetector. A schematic illustration of the OPM operation is shown in Figure 6.

Figure 6 Schematic illustration of the operation of an OPM. A zero-field environment (top) and an external magnetic field (bottom).

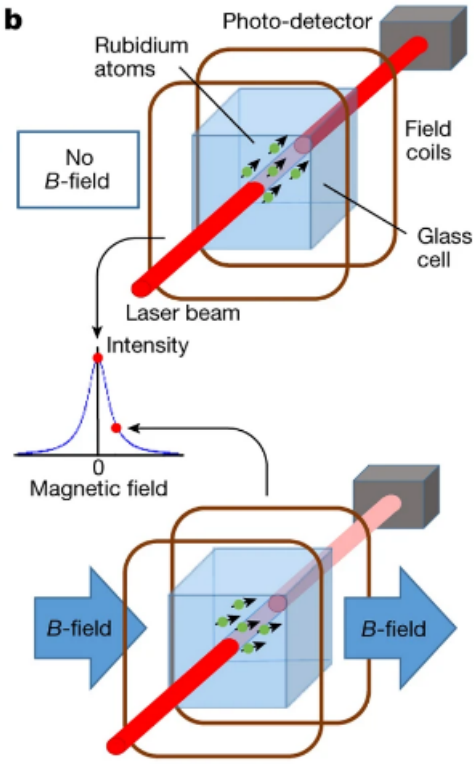

Reproduced from (BOTO et al., 2018)

Initially, OPMs were limited to measuring only two magnetic field components. Recently, triaxial OPMs were developed, bringing significant benefits. By measuring all three magnetic field components, these sensors offer greater information density without requiring additional sensors. Additionally, triaxial OPMs improved the measurement precision as they can internally remove cross-axis sensitivity. Lastly, with triaxial OPMs, spatial filtering algorithms can more efficiently remove external noise and interference. QuSpin, Inc. (Colorado, USA) has manufactured a triaxial OPM with the same size, weight, power, and cost as their dual-axis (QUSPIN INC, 2022). They reported a slight reduction in sensitivity of 7-12 $fT/Hz^{1/2}$ in single-axis mode, 10-15 $fT/Hz^{1/2}$ in dual-axis mode, and 15-20 $fT/Hz^{1/2}$ in tri-axis mode.

Over time, OPMs have been miniaturized to the point where they can be as small as 24.4 x 16.6 x 12.4 mm^2, such as the ones produced by QuSpin, Inc (Figure 7). This allows for the development of multi-channel systems that cover a large area of the body. Up to 49 OPMs were used in magnetoencephalography (MEG) studies to measure the magnetic field produced by electrical currents in the brain tissue (BORNA et al., 2017; HILL et al., 2020), and up to 16 OPMs in fMCG studies (ALEM et al., 2015; ESCALONA-VARGAS et al., 2020; STRAND et al., 2019). Measurements with such number of sensors are only possible if they are small and lightweight. In addition, OPMs can be placed closer to the body and in different arrangements that conform to the patient's body, enabling the detection of larger signals and field patterns with a higher spatial resolution (IIVANAINEN; STENROOS; PARKKONEN, 2017). This provides a more flexible option for a variety of measurement applications and can lead to improved accuracy in detecting and measuring magnetic fields. Finally, the small size of OPMs allows for the use of smaller magnetic shields, which can reduce the overall cost and complexity of the system (STRAND et al., 2019)

Figure 7 (A) Schematic illustration of the OPM's main components (electronics module, 6m long cable, and the sensor) with their respective dimensions. **(B)** Photograph of the OPM sensor next to a pen for size comparison.

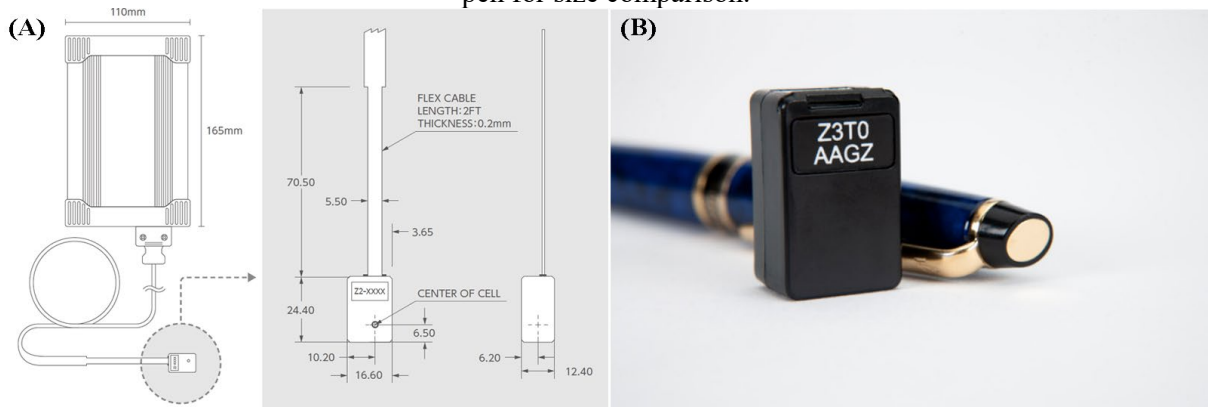

Reproduced from (QUSPIN INC, 2022)

1.5. Shielding

As the magnetic field from the fetal cardiac activity is weak, any other magnetic field source produces interference in the signal, such as nearby electronic equipment and other biological sources (Figure 8). For instance, the maternal cardiac magnetic field amplitude is typically ten times higher than the fetal. Also, the presence of the Earth's magnetic field can compromise the dynamic response of the sensors, as it is 10^6 times higher than the fetus' heart signal. Therefore, magnetic shields are used to reduce interference from external sources, allowing the recording of the magnetic field from the fetus' heart.

Figure 8 Magnetic flux density of environmental (blue) and biological (red) sources.

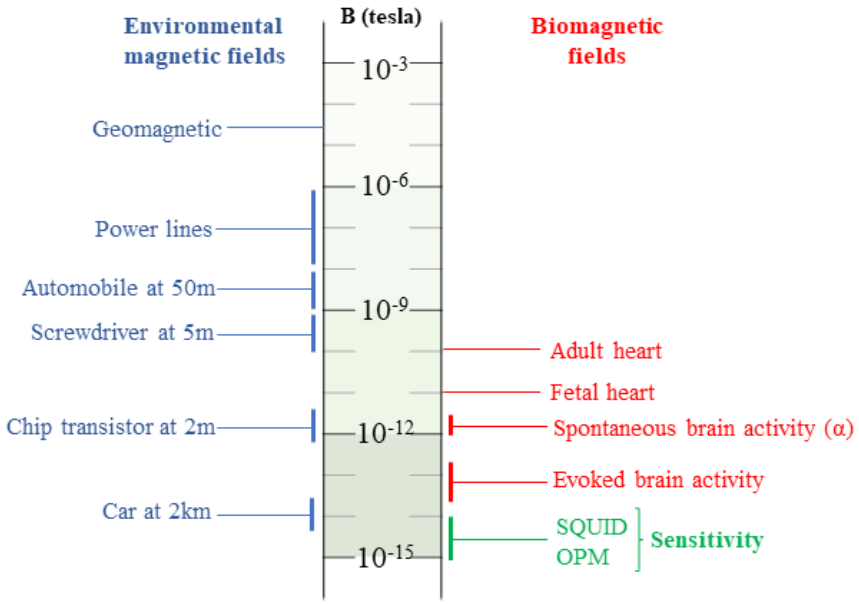

Adapted from (VOL, 2018)

There are two types of magnetic shielding (HASSELGREN; LUOMI, 1995). High-frequency magnetic fields can be shielded using highly conductive materials like copper and aluminum. When these materials are exposed to a magnetic field, eddy currents are generated within them, creating an opposing magnetic field that repels the external magnetic field. As a result, the external magnetic field is forced to travel parallel to the shield's wall (Figure 9A). In contrast, low-frequency magnetic fields are shielded using materials with high magnetic permeability, such as mu-metal. In this case, the material acts as a low reluctance path for the magnetic field lines, attracting them towards the shield and directing them through its wall. This prevents the magnetic field from passing through the shielded area (Figure 9B). Materials with high magnetic permeability are the most suitable for high-performance magnetic shielding in biomedical applications. Although mu-metal has exceptionally high permeability (μ = 80k-100k H/m), its low electrical resistivity ($\rho = 10^{-6}$ Ωm) generates magnetic noise due to thermal noise, which can be a limiting factor when the sensor is close to the shield (LEE; ROMALIS, 2008; MA et al., 2021). Recently, ferrite has been increasingly used as magnetic shielding because of its high magnetic permeability (μ = 5k H/m), high electrical resistivity (ρ = 1 Ωm), and negligible eddy current loss at low frequencies (<100 Hz) (FAN et al., 2020; FANG et al., 2022; KORNACK et al., 2007; PANG et al., 2022; YANG et al., 2022). (KORNACK et al., 2007) have shown that a 1 cm thick ferrite shield is equivalente to a 1 mm thick mu-metal shield of the same size, as the difference in magnetic permeability can be compensated by increasing

the thickness. Additionally, the noise of a ferrite shield is 25 times lower at 30 Hz than the mu-metal shield due to the absence of thermal noise.

Figure 9 (A) High electrical conductivity shield for high-frequency magnetic fields. **(B)** High magnetic permeability shield for low-frequency magnetic fields.

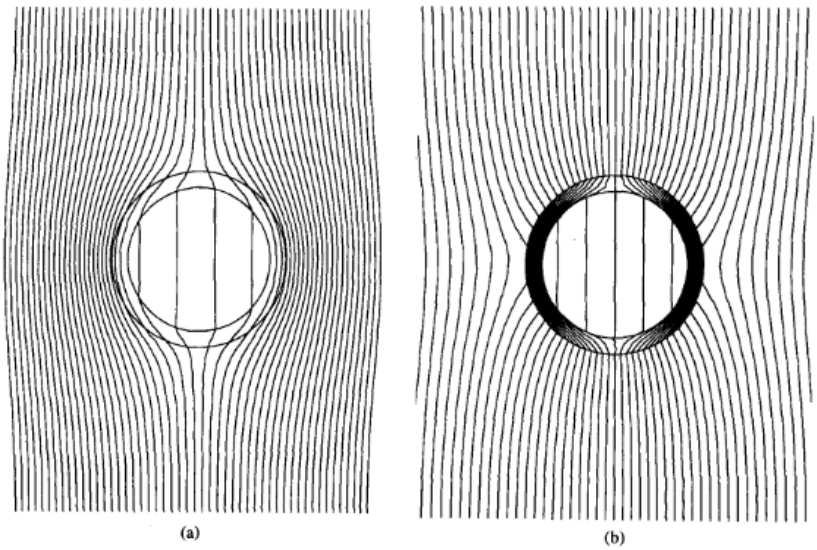

Reproduced from (HASSELGREN; LUOMI, 1995)

In addition to the material, the shape of the shield can also influence the shielding effectiveness. To achieve optimal shielding performance, spherical shields offer the most uniform effectiveness in all directions, but their complex manufacturing process and bulky size make them expensive. On the other hand, cubic shields can also provide shielding effectiveness equal in all directions and are simpler to manufacture. Still, they require more material and are generally larger, increasing their overall cost. Cylindrical shields are relatively easier to manufacture and often more cost-effective, although their shielding effectiveness in the transverse direction is greater than in the longitudinal direction (HASSELGREN; LUOMI, 1995; MAGER, 1970). A particular drawback of cylindrical shields is that, for biomedical purposes, one end of the cylinder must be kept open to prevent patient claustrophobia, which reduces the shielding factor, especially in the longitudinal direction.

In the past, SQUIDs were the only technology available for biomagnetic measurements, which required an MSR with large dimensions to house the Dewar, patient bed, and electronics. The high cost of these systems made them accessible only to specialized research centers. However, with the advent of OPMs, multilayer cylindrical shields slightly longer than a person could be used instead of MSR (BORNA et al., 2017; HE et al., 2019; STRAND et al., 2019). This new technology drastically reduced the cost while maintaining the same level of shielding effectiveness, particularly in the transverse directions. Therefore, studies have been conducted

to make this new OPM-based system within a person-sized cylindrical shield a low-cost alternative to SQUID-MSR.

In Figure 10 is possible to compare the difference in size between the SQUID-MSR system and the OPM within a person-sized shield for fMCG application. The photographs are from the systems installed in the Biomagnetism Laboratory at the University of Wisconsin-Madison. Figure 10A shows the SQUID in a 2-layer mu-metal MSR, while Figure 10B shows the 3-layer mu-metal person-sized cylindrical shield. An array of 11 OPMs is depicted in Figure 10C in comparison to the large size of the SQUID in Figure 10A. Figure 10D demonstrates the positioning of the patient for an fMCG measurement with OPMs within the person-sized shield.

Figure 10 Pictures taken from the system installed at the University of Wisconsin-Madison. **(A)** SQUID in a cubic MSR. **(B)** Person-sized cylindrical shield. **(C)** Patient positioning for OPM-fMCG in the person-sized shield.

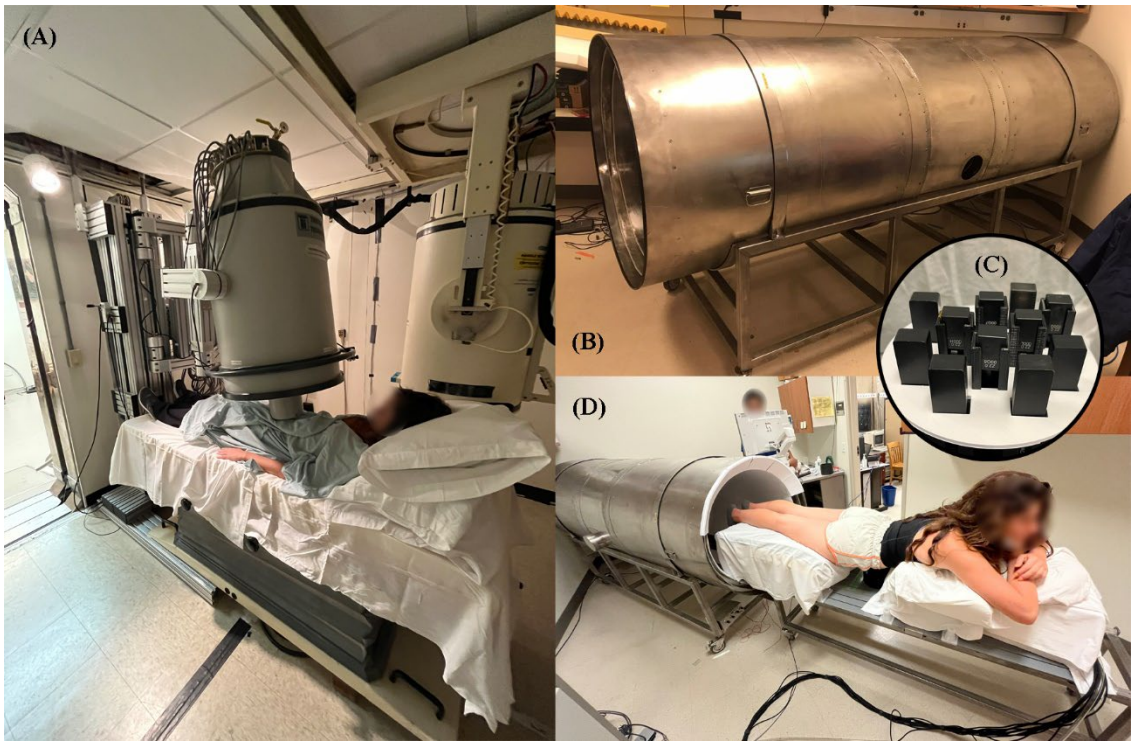

Elaborated by the author.

2. INTRODUCTION

fMCG has emerged as an important complementary diagnostic tool to fetal echocardiography and an alternative to fetal electrocardiography (STRASBURGER; CHEULKAR; WAKAI, 2008). Clinically, the most important application of fMCG is diagnosing fetal arrhythmia (STRASBURGER; CHEULKAR; WAKAI, 2008; WACKER-GUSSMANN et al., 2022), which was recently endorsed by the American Heart Association in its inaugural Statement on Diagnosis and Treatment of Fetal Cardiac Disease (DONOFRIO et al., 2014). The OPMs-based system within a person-sized cylindrical magnetic shield has made fMCG more practical. However, a significant limitation is that one end is kept open for patient comfort, which substantially reduces the shielding performance, especially in the longitudinal direction.

Several methods have been investigated to improve the shielding performance of open-ended person-sized shields. It is well known from simulations that lengthening the shield improves performance; however, this increases the cost and difficulty of finding suitable space in a clinical setting. Adding a fourth layer of shielding to a typical 3-layer person-sized shield can result in performance similar to that of a large-size MSR (HE et al., 2019), but again increases the cost and size of the shield. Another approach implemented by several groups (BORNA et al., 2017; XIA et al., 2006) is to add an extension that reduces the diameter of the opening to approximately 60 cm. This was demonstrated in simulations to improve the shielding by a factor of two and shift the optimal position toward the center of the shield (LABYT; SANDER; WAKAI, 2022). For fMCG, however, it is not feasible to appreciably narrow the opening. The diameter of the inner shield needs to be 75 cm or greater to allow a pregnant woman to enter comfortably. Lastly, the best shielding performance is achieved with superconducting shields (OHTA; MATSUI; UCHIKAWA, 2007), but the cost at the moment exceeds that of an MSR.

The problem of leakage interference from the shield opening is considerably more severe for fMCG than for other applications. For MEG and even MCG, the sensors can be positioned much closer to the closed than the open end of the shield. For fMCG, however, the sensors are placed near the middle of the shield. The leakage interference is especially strong in the longitudinal direction because, for cylindrical geometries, the shielding factor is approximately ten higher in the transverse than in the longitudinal direction. In the study of Strand and coworkers, the sensors were oriented to record only the transverse components of

the fMCG signal due to the low signal-to-noise ratio (SNR) of the longitudinal component (STRAND et al., 2019).

In this study, we investigated the use of a small ferrite shield to augment the performance of a conventional person-sized magnetic shield. Small ferrite shields have been used previously by Kornack and coworkers to circumvent Johnson noise associated with mu-metal shields (KORNACK et al., 2007). To our knowledge, our study is the first use of ferrite shields for a biomagnetism application. We show that the method is practical and provides a major benefit by allowing the longitudinal component of the fMCG to be recorded with a SNR similar to that of the transverse components.

Lastly, the appendix of this dissertation contains a study to which I contributed during my master's: "Magnetomechanical Fetal Cardiac Imaging: Feasibility of a New Multimodal Technique" (PHAN et al., 2022).

3. MATERIALS AND METHODS

3.1. Instrumentation

The measurements were performed within a cylindrical three-layer mu-metal shield (Amuneal Inc, Philadelphia, PA) of an inner diameter of 75 cm and length of 2.5 m (Figure 11A). One end of the shield was closed, and the other was kept open to avoid the risk of claustrophobia. It was placed on a custom-made support with a detachable extension that allows the patient's table to slide in and out of the shield.

The study took place at the Wisconsin Institute for Medical Research at the University of Wisconsin-Madison, where the earth's magnetic field is ≅ 54 μT. The residual field was reduced to approximately 10 nT by placing the shield perpendicular to the earth's magnetic field. A ferrite cylindrical shield (height 12.5 cm, inner diameter 15 cm, and thickness 1 cm) was placed inside the mu-metal shield with its axis perpendicular to the mu-metal shield's axis, as depicted in Figure 11. The ferrite shield has one end open and the other closed with a removable end cap of the same material and thickness, and 12 access holes allowing the cables to exit.

Three OPM sensor versions – Gen 1, Gen 2, and Gen 3 (QuSpin Zero Field Magnetometer, QuSpin Inc, Louisville, CO, USA) – were used to record the fMCG. The Gen 1 and Gen 2 sensors are dual-axis with intrinsic magnetic field resolution of 10-15 $fT/Hz^{1/2}$. Each sensor measures two orthogonal components of the magnetic field, one parallel to the long axis of the sensor (Z) and the other parallel to the short axis (Y). The Gen 2 sensors are smaller than the Gen 1 sensors. The Gen 3 sensors became available toward the end of the study. They are triaxial sensors (Z, Y, X) and have slightly lower magnetic field resolution. A 3D-printed plastic holder accommodated up to 12 OPM sensors arranged in an offset square grid pattern of 9×9 cm (Figure 11C). The sensors were oriented so that the Z and Y outputs recorded the magnetic field in the horizontal and vertical transverse directions of the mu-metal shield (Figure 11D), and the X component of the triaxial sensors recorded the magnetic field in the longitudinal direction. The signals were digitized at 1 kHz using a LabView data acquisition system (National Instruments, Austin, TX, USA). Signal processing was performed using a custom computer program written in Matlab (MathWorks Inc., Natick, MT, USA).

Figure 11 (A) Photograph showing the open-ended 3-layer mu-metal cylindrical shield, the sliding patient table, and the OPM sensors; **(B)** Photograph of the sidewall and bottom cap of the ferrite shield showing the sensors' access hole; **(C)** Photograph of the sensors distributed within the ferrite shield; **(D)** Diagram showing the directions with respect to the mu-metal shield. The longitudinal direction is defined by the long axis of the cylinder. The vertical transverse direction is perpendicular to the floor, and the horizontal transverse direction is parallel. The OPMs were oriented so that their Y and Z outputs record the magnetic field in the horizontal and vertical transverse directions, respectively, and the X output (Gen 3 sensors) records the magnetic field in the longitudinal direction.

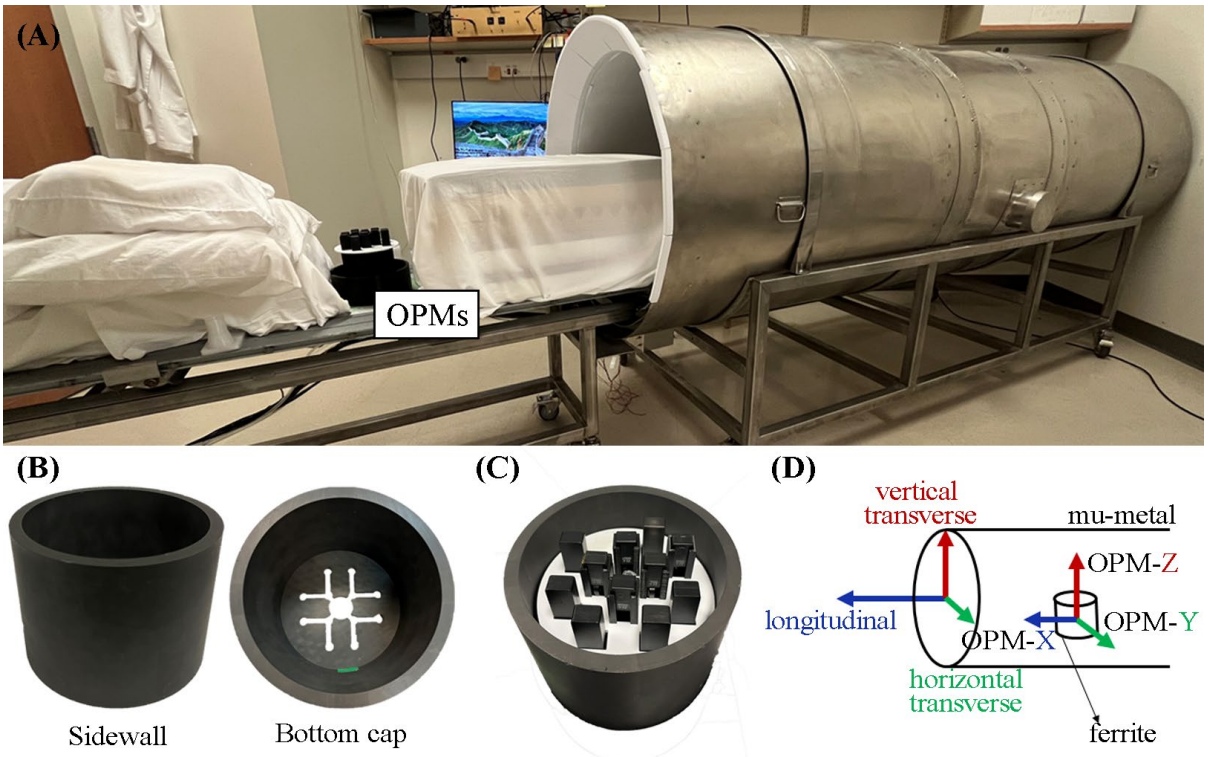

Elaborated by the author

3.1.1. Demagnetization

Ferromagnetic materials, such as mu-metal and ferrite, have the particular property of aligning their magnetic domains when subjected to a strong magnetic field. Some domains may not return to their original random state after the magnetic field is removed, leading to magnetization and, consequently, the production of an undesirable magnetic field (COLLINSON; CREE; RUNCORN, 1964). Therefore, it is important to maintain the magnetization level as low as possible.

Degaussing was performed in the ferrite shield by applying an alternating current through a solenoid, creating a rapidly changing magnetic field. The magnetic domains try to orient according to the magnetic field, but since it changes fast, they end up randomized (COLLINSON; CREE; RUNCORN, 1964; LOVEJOY, 1993). A small residual magnetic field may occur due to hysteresis; however, it should be small enough for the OPMs to work.

A variable transformer (variac; model TDGC2-ED, max output 30A, Circuit Specialists, Tempo, AZ, USA) was connected to a step-down transformer to vary the current and the magnetic field in small increments. First, a thick cable was wound axially around the ferrite shield's sidewall, and then radially. To demagnetize, the current in the transformer was gradually reduced from 20 A down to 0 A with decrements of a few amperes, and monitored with an ammeter. This process was repeated for the bottom cap of the shield. The magnetic noise level was monitored by analyzing the power spectra derived from 20-s environmental noise measurements with the OPMs. This process was repeated until the magnetic noise level inside the shield was as low as possible and all OPMs were working well.

3.2. Vertical Placement of Sensor Array Within Ferrite Shield

The vertical placement of the sensor array within the ferrite shield affects the shielding effectiveness and signal fidelity. If the sensors are positioned well below the top of the shield, the interference will be strongly attenuated, but the signal may also be diminished. If the sensors are placed near the top of the shield, the signal loss will be minimal, but the shielding effectiveness will also be reduced. To help determine an optimal placement, the shielding factor as a function of the vertical position of the sensor array with respect to the top of the ferrite shield was measured.

At a distance of 140 cm from the opening of the mu-metal shield, the sensors were suspended above the ferrite shield using a holder attached to a tripod. The ferrite shield, resting on a plastic lab jack, could be adjusted in height through a small access port in the sidewall of the mu-metal shield (Figure 12). Initially, with the ferrite shield at its lowest position, the OPMs were entirely outside the shield. However, as the height of the ferrite shield was increased, the OPMs gradually entered the shield. Magnetic field measurements were taken every few centimeters, each lasting for 30 s. Five dual-axis and four tri-axis OPMs were used to obtain the magnetic field in all three directions. To simulate environmental interference, a coil placed outside the mu-metal shield was used to generate a magnetic field at 23 Hz. The amplitude of the magnetic field was measured from the power spectrum. Lastly, the shielding factor was calculated as the ratio of the magnetic field in the absence of the ferrite shield to the field in the presence of the shield.

Figure 12 Schematic representation of the experimental setup to measure the shielding factor as a function of the vertical position of the sensor array to the ferrite shield opening

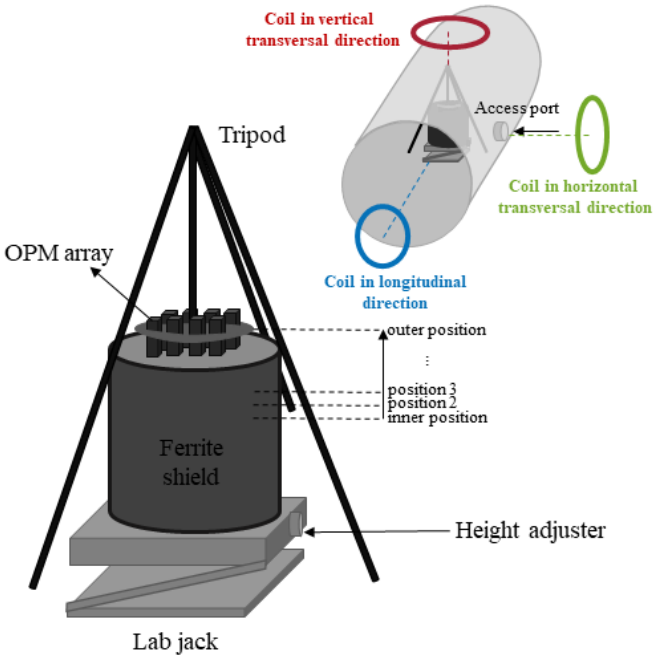

Elaborated by the author

3.3. Attenuation of Environmental Interference

The effectiveness of the ferrite shield in attenuating environmental interference was assessed by placing the center of the OPM array 140 cm from the shield opening and recording the interference with and without the ferrite shield. Five dual-axis and four tri-axis OPMs were used to obtain the noise in all three directions. Each measurement lasted 30 s. The power spectra for each direction in both cases were obtained using Welch's method in Matlab.

3.4. Human Studies

3.4.1. Subjects

The protocol was approved by the UW-Madison Health Sciences IRB, and informed consent was obtained from all subjects. The subjects were 10 adult pregnant women studied at 21-36 weeks gestation. Seven of the pregnancies were uncomplicated. One was complicated by fetal LQTS. A second was complicated by endocardial fibroelastosis and fetal AV block associated with iso-immune disease. A third involved a case of congenital heart disease, Tetralogy of Fallot.

3.4.2. Data collection

The data was collected with the mother lying prone on two sections of foam mattresses separated by a gap. The sensor array was covered by a thin piece of foam and placed within the gap, in contact with the mother's abdomen from below. Airflow was applied to the sensors to prevent them from overheating. After positioning the mother, the patient table was slid into the mu-metal shield for data collection. The sensor array was approximately 140 cm from the mu-metal shield opening. Two 60-s runs were recorded – one with and one without the ferrite shield.

3.4.3. Data processing

The performance of the ferrite shield was assessed by four parameters: the amplitude of the fetal and maternal QRS complexes (fQRS and mQRS, respectively), the amplitude of the environmental noise, and the SNR. The parameters were calculated separately for each sensor and direction.

To analyze the effect of the shield, the parameters must be measured from the raw signal. Thus, a 1-100 Hz band-pass filter was applied to remove the offset without removing the main interferences. The amplitude of each fQRS and mQRS was measured as the peak-to-peak amplitude. The environmental noise amplitude was defined as the root-mean-square of each interval between the end of one QRS complex and the beginning of the next. After excluding artifacts, all the fQRS, mQRS, and noise amplitudes throughout the signal were averaged, yielding one final value for each variable. Finally, the SNR was calculated as the average fQRS amplitude divided by the average noise amplitude.

3.4.4. Statistical analysis

We performed an ANOVA with a 2x2 factorial randomized block design where the patients were considered blocks (random effects). The presence of the shield and the direction, as well as the interaction between them, were considered fixed effects. All analyses were performed using the Mixed procedure of SAS.

4. RESULTS

4.1. Vertical Placement of Sensor Array Within Ferrite Shield

Figure 13 shows the shielding factor in each direction as a function of the vertical position of the sensor array with respect to the top of the ferrite shield. The shielding factors are modest in the transverse directions but substantial in the longitudinal direction. Although the shielding factors increase when the sensors are positioned farther within the shield, an additional, critically important consideration is the need to situate the sensors as close as possible to the fetal heart. This is difficult unless the sensors are near the top of the shield. Based on these considerations, we chose to position the OPM sensors so that the sensors were approximately 1.2 cm below the top of the ferrite shield. At this position, the shielding factors are 1.7, 15.5, and 9.6 in the vertical transverse, horizontal transverse, and longitudinal directions, respectively. Unfortunately, the positioning was constrained by the height of the OPM Gen 1, which is 11 cm, while the ferrite shield is 12.5 cm height. However, using only smaller OPMs, such as Gen 2 and Gen 3, allows for greater flexibility in selecting the appropriate height.

Figure 13 Shielding factor in each direction for different vertical positions of the sensor array with respect to the top/open end of the ferrite shield. Negative values indicate that the sensor array was above the top of the shield. The data was fitted in a curve, and the shielding factor obtained for the vertical transverse, horizontal transverse, and longitudinal directions was 1.7, 15.5, and 9.6, respectively.

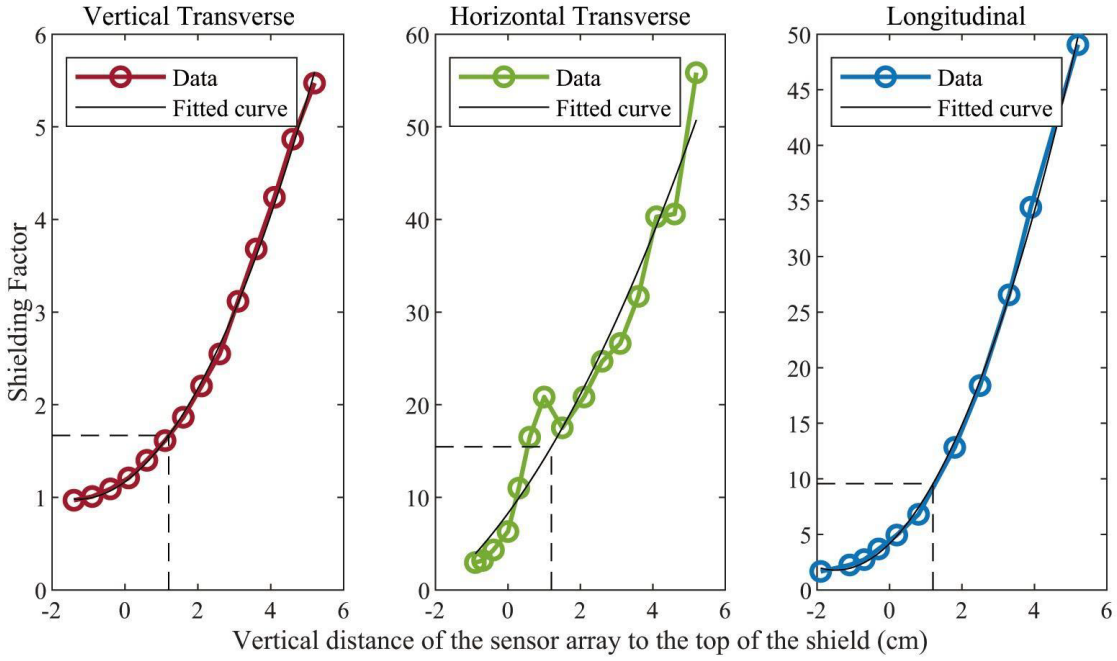

Elaborated by the author

4.2. Attenuation of Environmental Interference

Figure 14 shows the effect of the ferrite shield on the power spectra of the environmental magnetic noise components near the center of the mu-metal shield. As expected, in the absence of the ferrite shield, the longitudinal direction is much noisier than both transverse directions. When using the ferrite shield, the interference in all directions is significantly attenuated, but the degree of attenuation is much greater for the longitudinal direction. Thus, the ferrite shield compensates for the poorer performance of the mu-metal shield in the longitudinal direction so that the residual interference is similar in all directions.

Figure 14 Semilog plots of the power spectra of the environmental magnetic noise in three directions inside the mu-metal shield with (red) and without (black) the ferrite shield around the sensors.

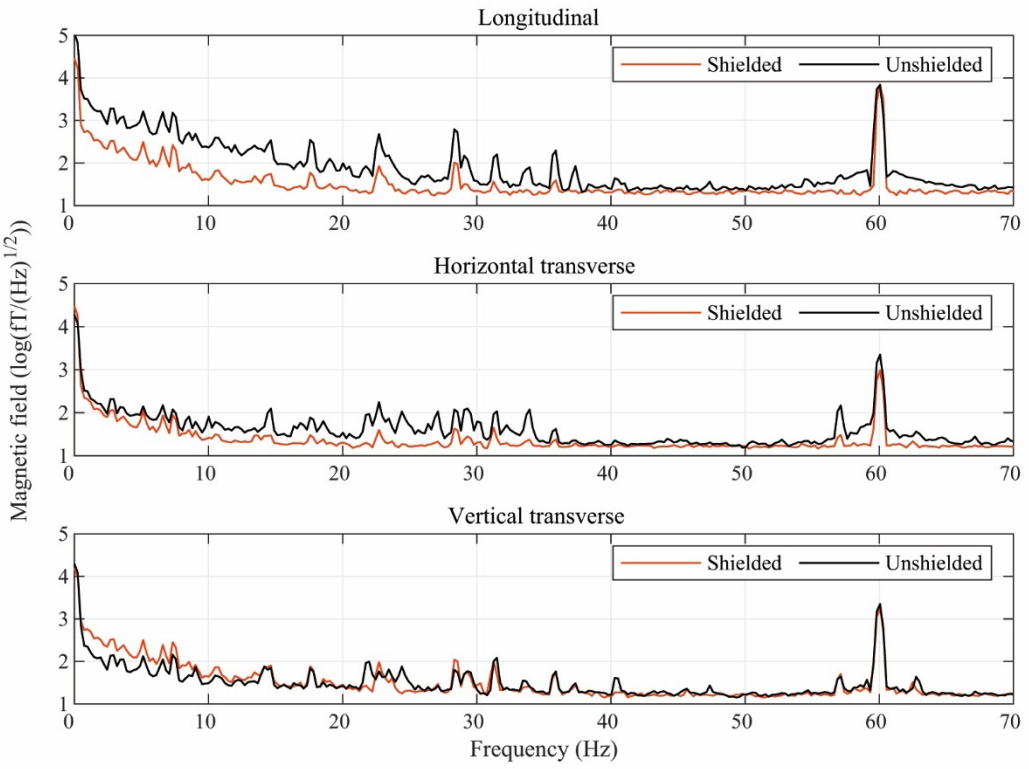

Elaborated by the author

4.3. Human studies

This effectiveness of the ferrite shield is clearly seen in the fMCG traces shown in Figure 15. Without the shield, the longitudinal component is completely dominated by noise. Although it was not possible to quantitatively compare the effect of the ferrite shield on longitudinal parameters, the improvement is evident when comparing the traces.

Figure 15 Effect of the ferrite shield in all components of two triaxial OPMs in fMCG recordings of a fetus with Tetralogy of Fallot in sinus rhythm. The strips are 1.2 seconds long and depict an average of 5s of fMCG. A signal filter was applied before averaging. Components of the fetal signal are represented by red (QRS), green (T-wave), magenta (U-wave), and orange (P-wave) asterisks.

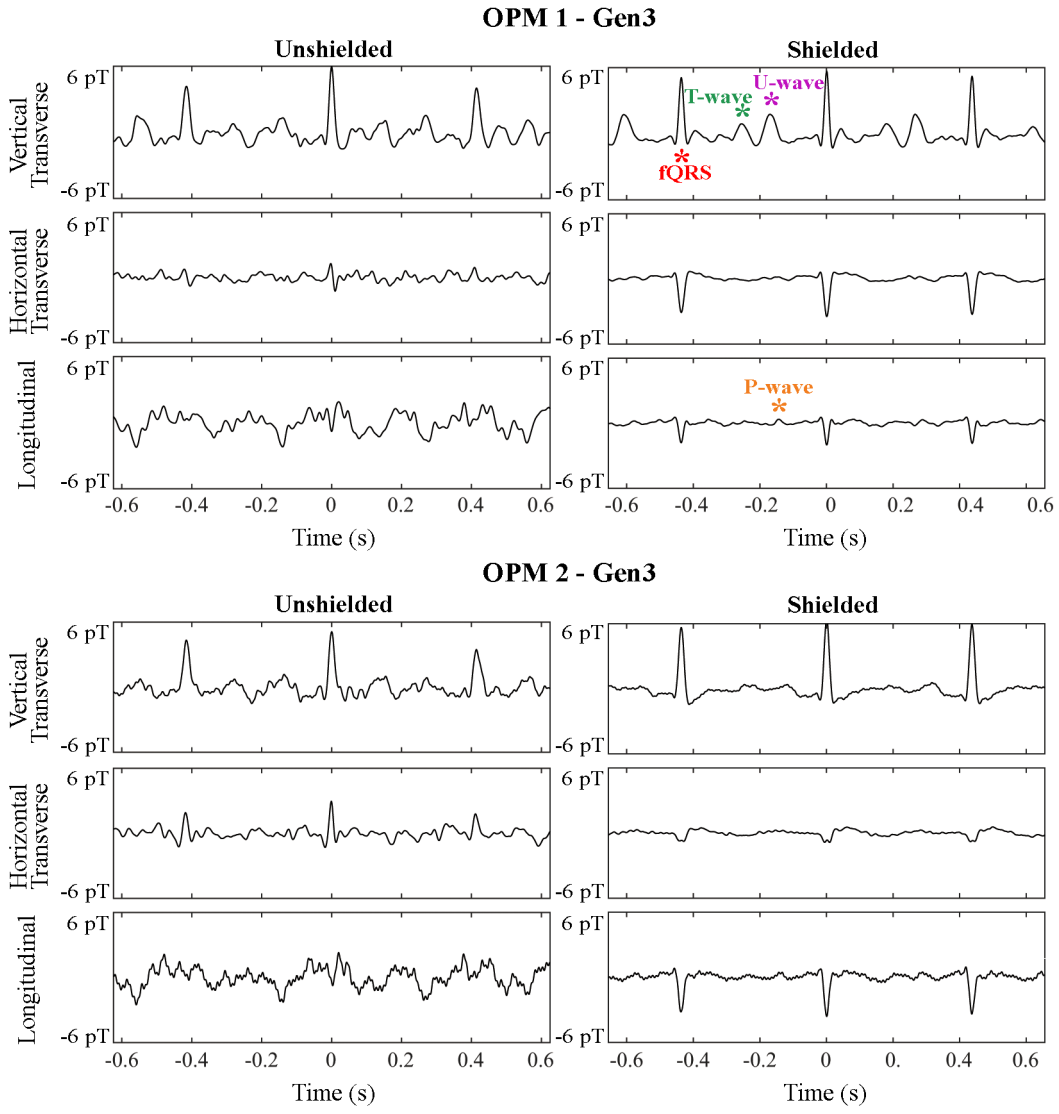

Elaborated by the author

Analysis and interpretation of the human data were complicated by several factors. The data show occasional inconsistencies and anomalies, such as greater than expected changes in signal amplitude between the shielded and unshielded data. We largely attribute this to the fact that removing the shield requires repositioning the subject, and changes in the position and orientation of the fetus between measurements can result in inconsistencies. Also, for reasons we do not completely understand, maternal interference was absent in both shielded and unshielded data for two patients, and it was present in the shielded data but absent in the unshielded data for one patient. Statistical analysis was performed only in the five cases where maternal interference was present in both unshielded and shielded data.

Table 1 presents the results of the statistical analyses. Using the ferrite shield affected all parameters ($p < 0.05$): the fQRS and mQRS amplitudes and the noise amplitude were reduced considerably, while the SNR increased significantly. The fQRS amplitude was reduced by 47% in the horizontal transverse direction and 32% in the vertical transverse direction, the mQRS amplitude was reduced by 47% and 29%, the noise was reduced by 55% and 47%, and the SNR increased by 32% and 24%, respectively. The direction did not affect the parameters, but the interaction between the presence of the shield and the direction was significant for the fQRS amplitude ($p = 0.034$). The multiple comparisons showed that after including the shield, the difference in horizontal and vertical transverse fQRS amplitude became significant (p = 0.033).

Table 1 Statistical results for fetal and maternal QRS amplitude (fQRS and mQRS, respectively), noise amplitude, and signal-to-noise ratio (SNR) for horizontal and vertical transverse directions, with and without the ferrite shield. The * indicated p-value < 0.05.

Variables	Effects				*p*-value		
	Horizontal Transverse		Vertical transverse				
	Unshielded	Shielded	Unshielded	Shielded	Shield	Direction	Shield x Direction
fQRS (pT)	20.8 ± 1.1	11.1 ± 1.1	19.8 ± 1.2	13.4 ± 1.2	<0.0001*	0.370	0.034*
mQRS (pT)	22.8 ± 1.3	12.1 ± 1.3	23.0 ± 1.3	16.4 ± 1.3	<0.0001*	0.072	0.098
Noise (pT)	8.0 ± 0.5	3.6 ± 0.5	7.1 ± 0.5	3.8 ± 0.5	<0.0001*	0.313	0.119
SNR	2.7 ± 0.2	3.6 ± 0.2	2.9 ± 0.2	3.6 ± 0.2	<0.0001*	0.081	0.313

In the rhythm strips in Figure 16, the fetus presents with a slow FHR due to complete heart block, while the mother shows a relatively high heart rate. Figures 16(A and B) show raw and signal-processed fMCG recordings obtained without the ferrite shield, while Figures 16(C and D) show recordings made with the ferrite shield. The results in Table 1 are compatible with the rhythm strips in Figure 16. The raw fMCG shows that the fQRS, mQRS, and noise amplitudes were reduced by the ferrite shield. The processed fMCG shows that after applying signal processing to remove interferences, fetal T-waves (green asterisks) could be resolved with the ferrite shield. Also, maternal interference was completely removed when using the ferrite shield but was visible (blue asterisks) in the unshielded fMCG tracings.

Figure 17 shows averaged waveforms from fMCG recordings of a healthy fetus. Although signal processing techniques were applied to obtain the final waveform, it is evident that the SNR improved with the use of the ferrite shield, and the P- and T-wave components of the fMCG were better resolved.

Figure 16 Effect of the ferrite shield around the OPMs in fMCG recordings of a fetus with complete heart block and mother with high heart rate. The rhythm strips are 5 seconds in duration. A significant reduction in maternal QRS and noise amplitude (blue asterisks) and a slight reduction in fetal QRS (red) are observed in the raw rhythm in (**A, C**). The filtered rhythm in (**B, D**) shows that, with the ferrite shield, the maternal interference was completely gone, and the fetal T-wave (green) was resolved.

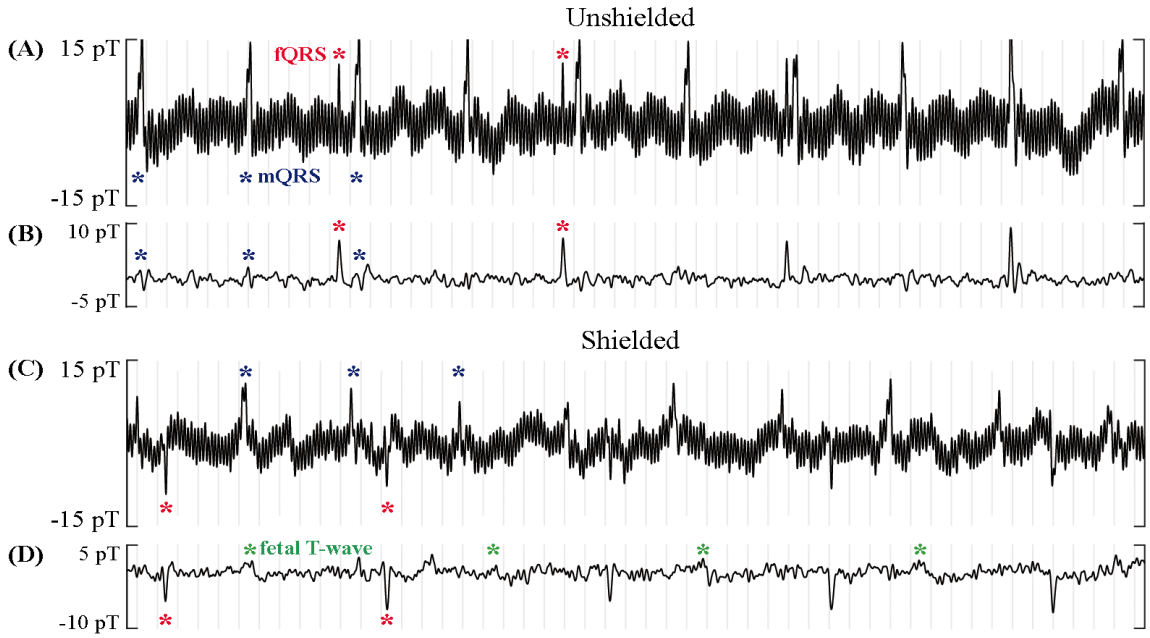

Elaborated by the author.

Figure 17 Average waveform of fMCG recordings of a normal fetus in the absence (left) and presence (right) of the ferrite shield around the array of OPMs. The presence of the ferrite shield improves the resolution of the smaller fMCG components (P- and T-wave).

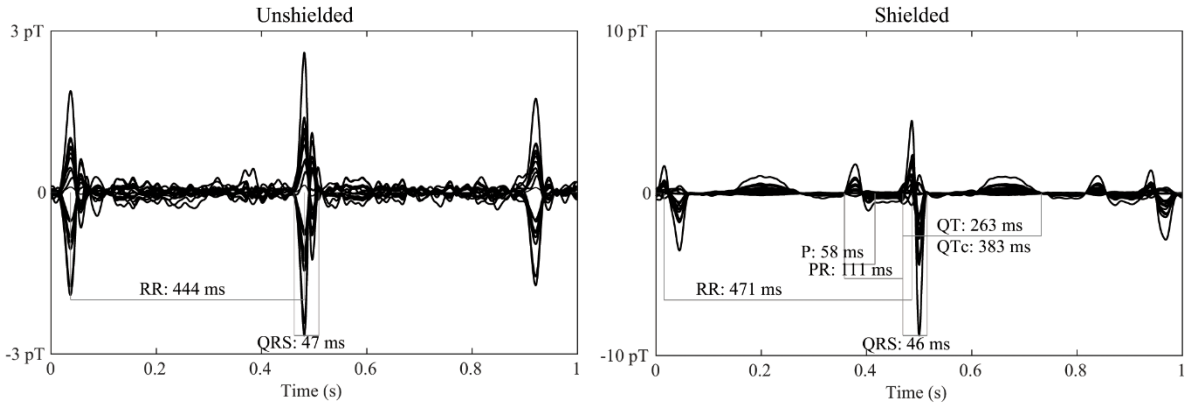

Elaborated by the author

5. DISCUSSION

In this study, we showed that placing an OPM array within a small ferrite shield can significantly improve the performance of OPM-based fMCG systems that use person-sized magnetic shields. The improvement results because the ferrite shield overcomes a main weakness of cylindrical mu-metal shields; namely, the low shielding factor along the longitudinal direction. As expected, the performance improvement is modest in the transverse directions but substantial in the longitudinal direction. For this reason, the shield is especially helpful when using triaxial OPM sensors, which recently have become commercially available. These sensors allow all three components of the magnetic signal to be recorded at the same location. In general, the signal components are independent, and it is necessary to measure all three to extract all the information available in the signal. This is problematic using cylindrical person-sized shields due to the low shielding factor in the longitudinal direction; however, as demonstrated here, the ferrite shield can compensate for this shortcoming, allowing all three channels of the triaxial output to exhibit similarly high SNR. In a prior study utilizing dual-axis OPMs, we oriented the sensors to measure only the transverse components (STRAND et al., 2019). This provided signals with high SNR at the expense of measurement of the longitudinal signal component. When using dual-axis OPMs, the ferrite shield allows flexible placement of the sensors, enabling both the transverse and longitudinal signal components to be measured. This provides a more complete characterization of the signal.

In some subjects, the increase in the signal quality resulting from the use of the ferrite shield provided significantly improved resolution of the P- and T-waves. These small waveform components are crucial to rhythm assessment. The differential diagnosis of most bradycardias and supraventricular tachycardias is based on the relative timing of the atrial and ventricular activations represented by the P-wave and QRS complex. Detection of repolarization abnormalities, such as QTc prolongation in long QT syndrome or ST segment changes due to ischemia, requires resolution of the T-wave. Thus, the technical improvements demonstrated in this study can provide a meaningful increase in diagnostic capability and may allow fMCG to be performed at earlier gestational ages.

A particular advantage of our method is the attenuation of maternal interference, which is the dominant interference in fMCG recordings. Typically, it is not possible to shield the sensors from maternal interference and other biological interferences emanating from the subject. Instead, signal processing is relied upon. The most effective methods utilize spatial

filtering, such as independent component analysis (ICA). In many cases, however, ICA cannot cleanly separate the fetal and maternal signals because their spatial characteristics, i.e., signal topographies, are not sufficiently distinct. This results in loss of fetal signal or incomplete removal of maternal interference, depending on the design of the filter. The ferrite shield can mitigate this problem by attenuating maternal interference and/or altering its spatial characteristics to improve the ability of the spatial filter to distinguish it from the fetal signal.

An additional advantage of the shield is improved signal visualization during data acquisition. While signal processing is highly effective in enhancing signal resolution, it cannot be performed in real-time. In addition to significant computation time, many signal processing methods require user input. Visualization of the signal during data acquisition is especially important for clinical application because it is critical to ensure that the quality and quantity of data are adequate before the patient leaves the lab.

Despite our focus on fMCG, the ferrite shield is potentially useful for other biomagnetism measurements. As discussed above, it can help isolate the signal of interest from sources of biological, as well as environmental, interference. For instance, it can attenuate maternal and fetal cardiac interferences in fetal MEG, and cardiac interference in magnetogastography and magnetoenterography studies. A recently demonstrated technique of simultaneously recording fMCG and fetal echocardiography (PHAN et al., 2023) – magnetomechanical imaging – can also benefit from the ferrite shield to attenuate interferences from the ultrasound probe. This may allow simultaneous, real-time display of fMCG and pulsed Doppler and other echocardiography modalities by connecting the fMCG to the ECG input of the ultrasound scanner. A significant limitation of the technique, however, is signal attenuation and/or distortion of the signal topography by the ferrite shield. These effects are relatively small and inconsequential for fMCG, which utilizes the temporal information in the signals; however, they are likely unacceptable for source localization applications, which require highly accurate modeling of the signal topography.

The ferrite shield is a practical and cost-effective method of improving signal quality in comparison to alternative methods of enhancing shielding performance mentioned in Introduction. It is simple and versatile. It can be used in conjunction with nearly any existing shield and can be easily put in place and removed as needed. Subjects report that the small ferrite shield structure helps distribute the pressure on the abdomen and is more comfortable than without it. A straightforward means of further improving the effectiveness of the method

is to add a second layer of shielding. Mu-metal is much more widely used for magnetic shielding than ferrite because mu-metal is cheaper and has higher magnetic permeability. This suggests the construction of a two-layer shield using ferrite for the inner shield and mu-metal for the outer shield, as implemented by (KORNACK et al., 2007).

6. CONCLUSION

In conclusion, we demonstrated the use of a small ferrite shield as a simple, practical method of overcoming the high level of environmental interference present in fMCG recordings made using person-sized magnetic shields. The method allows users to take full advantage of newly available OPM sensors that record all three components of the signal and provides meaningful improvements in signal resolution and diagnostic capability.

7. FINAL REMARKS

This dissertation is the result of a collaboration between the University of São Paulo and the University of Wisconsin-Madison. The study presents an innovative solution to enhance the performance of an OPM-based system within a person-sized cylindrical shield for fMCG measurements. This system was introduced by the research group at the University of Wisconsin-Madison as a low-cost option to the conventional SQUID in an MSR system. It represents a leap forward into making the fMCG technique widely accessible in healthcare facilities worldwide. Every improvement made to this system brings us closer to achieving this goal. However, there is a trade-off between improving the technique and increasing the cost and complexity. Therefore, the ferrite shield is a practical, simple, and versatile solution that enhances the signal resolution and diagnostic capability of the OPM-fMCG system without significantly increasing its cost.

Through this collaboration, we were able to install the first OPM-fMCG system within a person-sized shield in Brazil. The system is in the Biomagnetism Laboratory of the University of São Paulo in Ribeirão Preto (Figure 18). The activities undertaken during this project provided valuable experience, knowledge, and skills, enabling us to successfully develop and install a system that comprises an array of seven dual-axis OPMs within a three-layer mu-metal cylindrical shield, with an outer rectangular layer of aluminum, and cancellation coils in all three directions.

Our long-term goal is to establish ourselves as a reference center for diagnosing fetal arrhythmias using fMCG in Brazil. Additionally, we aim to explore the potential of this system in other applications, such as magnetogastrography, magnetoenterography, and beyond. With the installation of this system, we hope to make significant contributions to the field of biomagnetism research and clinical practice and ultimately improve healthcare outcomes for patients.

Figure 18 Person-sized magnetic shield installed in the Biomagnetism Laboratory at the University of São Paulo in Ribeirão Preto.

Elaborated by the author.

8. REFERENCES

ADLER, L. C.; FREEBORN, D.; TREVINO, H. M. **Blood Circulation in the Fetus and Newborn**. Disponível em: <https://www.urmc.rochester.edu/encyclopedia/content.aspx?ContentTypeID=90&ContentID=P02362>. Acesso em: 27 mar. 2023.

ALEM, O. et al. Fetal magnetocardiography measurements with an array of microfabricated optically pumped magnetometers. **Physics in Medicine and Biology**, v. 60, n. 12, p. 4797–4811, 21 jun. 2015.

BELL, W. E.; BLOOM, A. L. Optical Detection of Magnetic Resonance in Alkali Metal Vapor. **Physical Review**, v. 107, n. 6, p. 1559–1565, 1957.

BETTS, J. G. et al. **Anatomy & Physiology**. Houston: OpenStax College, Rice University, 2017.

BORNA, A. et al. A 20-channel magnetoencephalography system based on optically pumped magnetometers. **Physics in Medicine and Biology**, v. 62, n. 23, p. 8909–8923, 10 nov. 2017.

BOTO, E. et al. Moving magnetoencephalography towards real-world applications with a wearable system. **Nature**, v. 555, n. 7698, p. 657–661, 29 mar. 2018.

CLIFFORD, G. D. et al. Non-invasive fetal ECG analysis. **Physiological Measurement**, v. 35, n. 8, p. 1521–1536, 1 ago. 2014.

COHEN, D.; EDELSACK, E. A.; ZIMMERMAN, J. E. Magnetocardiograms taken inside a shielded room with a superconducting point-contact magnetometer. **Applied Physics Letters**, v. 16, n. 7, p. 278–280, abr. 1970.

COLLINSON, D.; CREE, K.; RUNCORN, S. **Methods in Palaeomagnetism**. 1st. ed. London: Elsevier, 1964.

CROTTI, L. et al. Long QT syndrome-associated mutations in intrauterine fetal death. **JAMA**, v. 309, n. 14, p. 1473–1482, 10 abr. 2013.

CUNEO, B. F. et al. Conduction System Disease in Fetuses Evaluated for Irregular Cardiac Rhythm. **Fetal Diagnosis and Therapy**, v. 21, n. 3, p. 307–313, 2006.

CUNEO, B. F. et al. In utero diagnosis of long QT syndrome by magnetocardiography. **Circulation**, v. 128, n. 20, p. 2183–2191, 12 nov. 2013.

CUNEO, B. F.; STRASBURGER, J. F.; WAKAI, R. T. The natural history of fetal long QT syndrome. **Journal of Electrocardiology**, v. 49, n. 6, p. 807–813, 1 nov. 2016.

DEHMELT, H. G. Modulation of a Light Beam by Precessing Absorbing Atoms. **Physical Review**, v. 105, n. 6, p. 1924–1925, 15 mar. 1957.

DONOFRIO, M. T. et al. Diagnosis and treatment of fetal cardiac disease: A scientific statement from the american heart association. **Circulation**, v. 129, n. 21, p. 2183–2242, 27 maio 2014.

DUPONT-ROC, J.; HAROCHE, S.; COHEN-TANNOUDJI, C. Detection of very weak magnetic fields (10−9gauss) by 87Rb zero-field level crossing resonances. **Physics Letters A**, v. 28, n. 9, p. 638–639, fev. 1969.

ESCALONA-VARGAS, D. et al. Recording and quantifying fetal magnetocardiography signals using a flexible array of optically-pumped magnetometers. **Physiological Measurement**, v. 41, n. 12, 1 dez. 2020.

FAGALY, R. L. Superconducting quantum interference device instruments and applications. **Review of Scientific Instruments**, v. 77, n. 10, 2006.

FAN, W. et al. Performance of Low-Noise Ferrite Shield in a K-Rb-21Ne Co-Magnetometer. **IEEE Sensors Journal**, v. 20, n. 5, p. 2543–2549, 1 mar. 2020.

FANG, X. et al. A High-Performance Magnetic Shield with MnZn Ferrite and Mu-Metal Film Combination for Atomic Sensors. **Materials**, v. 15, n. 19, 1 out. 2022.

HALL, J. E.; GUYTON, A. C. **Guyton and Hall: Textbook of Medical Physiology**. 12th. ed. Philadelphia: Saunders Elsevier, 2017. v. 8

HAPPER, W.; TANG, H. Spin-Exchange Shift and Narrowing of Magnetic Resonance Lines in Optically Pumped Alkali Vapors. **Physical Review Letters**, v. 31, n. 5, p. 273–276, 30 jul. 1973.

HASSELGREN, L.; LUOMI, J. Geometrical Aspects of Magnetic Shielding at Extremely Low Frequencies. **IEEE Transactions on Eletromagnetic Compatibility**, v. 37, n. 3, p. 409, 1995.

HE, K. et al. A high-performance compact magnetic shield for optically pumped magnetometer-based magnetoencephalography. **Review of Scientific Instruments**, v. 90, n. 6, 1 jun. 2019.

HILL, R. M. et al. Multi-channel whole-head OPM-MEG: Helmet design and a comparison with a conventional system. **NeuroImage**, v. 219, 1 out. 2020.

HIRSH, D.; SOUTHMAYD, G. Approach to ECG Interpretation. Em: **Handbook of Inpatient Cardiology**. Switzerland: Springer, 2020. p. 469–486.

HORNBERGER, L. K. Echocardiography assessment of fetal arrhythmias. **Heart**, v. 93, n. 11, p. 1331–1333, nov. 2007.

HORNBERGER, L. K.; SAHN, D. J. Rhythm abnormalities of the fetus. **Heart**, v. 93, n. 10, p. 1294–1300, 1 out. 2007.

HYETT, J. A. et al. Fetal heart rate in trisomy 21 and other chromosomal abnormalities at 10-14 weeks of gestation. **Ultrasound in Obstetrics and Gynecology**, v. 7, n. 4, p. 239–244, 1 abr. 1996.

IIVANAINEN, J.; STENROOS, M.; PARKKONEN, L. Measuring MEG closer to the brain: Performance of on-scalp sensor arrays. **NeuroImage**, v. 147, p. 542–553, 15 fev. 2017.

KÄHLER, C. et al. Fetal magnetocardiography in the investigation of congenital heart defects. **Early Human Development**, v. 69, p. 65–75, 2002.

KARINIEMI, V. et al. The fetal magnetocardiogram. **Journal of Perinatal Medicine**, v. 2, n. 3, p. 214–216, jan. 1974.

KHLER, C. et al. Fetal magnetocardiography: Development of the fetal cardiac time intervals. **Prenatal Diagnosis**, v. 22, n. 5, p. 408–414, 2002.

KOMINIS, I. K. et al. A subfemtotesla multichannel atomic magnetometer. **Nature**, v. 422, n. 6932, p. 596–599, 10 abr. 2003.

KORNACK, T. W. et al. A low-noise ferrite magnetic shield. **Applied Physics Letters**, v. 90, n. 22, p. 223501, 28 maio 2007.

LABYT, E.; SANDER, T.; WAKAI, R. **Flexible High Performance Magnetic Field Sensors**. Cham: Springer International Publishing, 2022.

LEE, S.-K.; ROMALIS, M. V. Calculation of Magnetic Field Noise from High-Permeability Magnetic Shields and Conducting Objects with Simple Geometry. **Journal of Applied Physics**, v. 103, p. 084904, 17 set. 2008.

LEEUWEN, P. VAN et al. Fetal heart rate variability and complexity in the course of pregnancy. **Early Human Development**, v. 54, p. 259–269, 1999.

LIAO, A. W. et al. Fetal heart rate in chromosomally abnormal fetuses. **Ultrasound in Obstetrics and Gynecology**, v. 16, n. 7, p. 610–613, dez. 2000.

LOVEJOY, D. Demagnetization. Em: **Magnetic Particle Inspection: A Practical Guide**. London: Kluwer Academic Publishers, 1993. p. 149–169.

MA, D. et al. Magnetic noise calculation of mu-metal shields at extremely low frequencies for atomic devices. **Journal of Physics D: Applied Physics**, v. 54, n. 2, 1 jan. 2021.

MAGER, A. J. Magnetic Shields. **IEEE Transactions on Magnetics**, v. 6, n. 1, p. 67–75, 1970.

MARIA, C. DI et al. The feasibility of long-term fetal heart rate monitoring in the home environment using maternal abdominal electrodes. **Physiological Measurement**, v. 16, p. 195–202, 1995.

MATTA, M. J.; CUNEO, B. F. Doppler Echocardiography for Managing Fetal Cardiac Arrhythmia. **Clinical Obstetrics & Gynecology**, v. 53, n. 4, p. 899–914, dez. 2010.

OHTA, H.; MATSUI, T.; UCHIKAWA, Y. A whole-head SQUID system in a superconducting magnetic shield. **IEEE Transactions on Applied Superconductivity**, v. 17, n. 2, p. 730–733, jun. 2007.

OLDENBURG, J. T.; MACKLIN, M. Changes in the conduction of the fetal electrocardiogram to the maternal abdominal surface during gestation. **American Journal of Obstetrics and Gynecology**, v. 129, n. 4, p. 425–433, out. 1977.

PANG, H. et al. Analysis and Suppression of Thermal Magnetic Noise of Ferrite in the SERF Co-Magnetometer. **Materials**, v. 15, n. 19, p. 6971, 7 out. 2022.

PETERS, M. J.; STINSTRA, J. G.; UZUNBAJAKAU, S. Fetal Magnetocardiography. Em: LIN, J. C. (Ed.). **Advances in Electromagnetic Fields in Living Systems**. Chicago: Springer, 2005. v. 4p. 1–40.

PHAN, T. et al. Magnetomechanical fetal cardiac imaging: Feasibility of a new multimodal technique. **Heart Rhythm**, 22 dez. 2022.

PHAN, T. et al. Magnetomechanical fetal cardiac imaging: Feasibility of a new multimodal technique. **Heart Rhythm**, 1 abr. 2023.

PIERI, J. F. et al. Compact long-term recorder for the transabdominal foetal and maternal elect rocard iog ram. **Med. Biol. Eng. Comput**, v. 39, p. 118–125, 2001.

QUSPIN INC. **QuSpin: An atomic devices company**. Disponível em: <https://quspin.com>. Acesso em: 5 mar. 2023.

REMPEN, A. Diagnosis of viability in early pregnancy with vaginal sonography. **Journal of Ultrasound in Medicine**, v. 9, n. 12, p. 711–716, dez. 1990.

ROBINSON, H. P.; SHAW-DUNN, J. Fetal heart rate as determined by sonar in early pregnancy. **BJOG: An International Journal of Obstetrics and Gynaecology**, v. 80, n. 9, p. 805–809, set. 1973.

SCHWARTZ, P. J. Stillbirths, sudden infant deaths, and long-QT syndrome: Puzzle or mosaic, the pieces of the jigsaw are being fitted together. **Circulation**, v. 109, n. 24, p. 2930–2932, 22 jun. 2004.

SHAH, V. et al. Subpicotesla atomic magnetometry with a microfabricated vapour cell. **Nature Photonics**, v. 1, n. 11, p. 649–652, nov. 2007.

SHAH, V. K.; WAKAI, R. T. A compact, high performance atomic magnetometer for biomedical applications. **Physics in Medicine and Biology**, v. 58, n. 22, p. 8153–8161, 21 nov. 2013.

SIMPSON, J. M.; YATES, R. W.; SHARLAND, G. K. Irregular heart rate in the fetus - Not always benign. **Cardiology in the Young**, v. 6, n. 1, p. 28–31, 1996.

STINSTRA, J. et al. Multicentre study of fetal cardiac time intervals using magnetocardiography. **BJOG: An International Journal of Obstetrics and Gynaecology**, v. 109, n. 11, p. 1235–1243, 1 nov. 2002.

STRAND, S. et al. Low-Cost Fetal Magnetocardiography: A Comparison of Superconducting Quantum Interference Device and Optically Pumped Magnetometers. **Journal of the American Heart Association**, v. 8, n. 16, 20 ago. 2019a.

STRAND, S. et al. Low-Cost Fetal Magnetocardiography: A Comparison of Superconducting Quantum Interference Device and Optically Pumped Magnetometers. **Journal of the American Heart Association**, v. 8, n. 16, 20 ago. 2019b.

STRAND, S. A.; STRASBURGER, J. F.; WAKAI, R. T. Fetal magnetocardiogram waveform characteristics. **Physiological Measurement**, v. 40, n. 3, 22 mar. 2019.

STRASBURGER, J. F.; CHEULKAR, B.; WAKAI, R. T. Magnetocardiography for fetal arrhythmias. **Heart Rhythm**, v. 5, n. 7, p. 1073–1076, jul. 2008.

STRASBURGER, J. F.; CHEULKAR, B.; WICHMAN, H. J. Perinatal Arrhythmias: Diagnosis and Management. **Clinics in Perinatology**, v. 34, n. 4, p. 627–652, dez. 2007.

STRASBURGER, J. F.; WAKAI, R. T. Fetal cardiac arrhythmia detection and in utero therapy. **Nature Reviews Cardiology**, v. 7, n. 5, p. 277–290, maio 2010.

TAYLOR, M. J. O. et al. Non-invasive fetal electrocardiography in singleton and multiple pregnancies. **BJOG: An International Journal of Obstetrics and Gynaecology**, v. 110, n. 7, p. 668–678, jul. 2003.

TIERNEY, T. M. et al. Optically pumped magnetometers: From quantum origins to multi-channel magnetoencephalography. **NeuroImage**, v. 199, p. 598–608, 1 out. 2019.

VOL, A. The Role of the Chemically Induced Polarization of Nuclei in Biology. **SPG BioMed**, 2018.

WACKER-GUSSMANN, A. et al. Fetal arrhythmias associated with cardiac rhabdomyomas. **Heart Rhythm**, v. 11, n. 4, p. 677–683, 2014.

WACKER-GUSSMANN, A. et al. Fetal atrial flutter: Electrophysiology and associations with rhythms involving an accessory pathway. **Journal of the American Heart Association**, v. 5, n. 6, 1 jun. 2016.

WACKER-GUSSMANN, A. et al. Contribution of Fetal Magnetocardiography to Diagnosis, Risk Assessment, and Treatment of Fetal Arrhythmia. **Journal of the American Heart Association**, v. 11, n. 15, 2 ago. 2022.

WACKER-GUSSMANN, A.; STRASBURGER, J. F.; WAKAI, R. T. Fetal Magnetocardiography Alters Diagnosis and Management in Fetal Congenital Heart Disease and Cardiomyopathy. **JACC: Clinical Electrophysiology**, v. 8, n. 9, p. 1159–1161, set. 2022.

WAKAI, R. T. et al. Magnetocardiographic rhythm patterns at initiation and termination of fetal supraventricular tachycardia. **Circulation**, v. 107, n. 2, p. 307–312, 21 jan. 2003.

WAKAI, R. T. Assessment of fetal neurodevelopment via fetal magnetocardiography. **Experimental Neurology**, v. 190, n. SUPPL. 1, p. 65–71, 2004.

WAKAI, R. T.; LENGLE, J. M.; LEUTHOLD, A. C. Transmission of electric and magnetic foetal cardiac signals in a case of ectopia cordis: the dominant role of the vernix caseosa. **Phys. Med. Biol**, v. 45, p. 1989–1995, 2000.

WIGGINS, D. L. et al. Magnetophysiologic and echocardiographic comparison of blocked atrial bigeminy and 2:1 atrioventricular block in the fetus. **Heart Rhythm**, v. 10, n. 8, p. 1192–1198, ago. 2013.

XIA, H. et al. Magnetoencephalography with an atomic magnetometer. **Applied Physics Letters**, v. 89, n. 21, 2006.

YANG, K. et al. Minimizing magnetic fields of the low-noise MnZn ferrite magnetic shield for atomic magnetometer. **Journal of Physics D: Applied Physics**, v. 56, n. 1, 6 jan. 2022.

ZHAO, H. et al. Simultaneity of foetal heart rate acceleration and foetal trunk movement determined by foetal magnetocardiogram actocardiography. **Physics in Medicine & Biology**, v. 47, p. 839–846, 2002.

ZHAO, H. et al. Fetal Cardiac Repolarization Abnormalities. **American Journal of Cardiology**, v. 98, n. 4, p. 491–496, 15 ago. 2006.

ZHAO, H. et al. Electrophysiological Characteristics of Fetal Atrioventricular Block. **Journal of the American College of Cardiology**, v. 51, n. 1, p. 77–84, 1 jan. 2008.

ZIZZO, A. R. et al. Fetal Heart Rate Variability Is Affected by Fetal Movements: A Systematic Review. **Frontiers in Physiology**, v. 11, 30 set. 2020.

9. APPENDIX - Magnetomechanical Fetal Cardiac Imaging: Feasibility of a New Multimodal Technique

This research letter is published at the journal Heart Rhythm (DOI: 10.1016/j.hrthm.2022.12.02). The reuse of this article in my thesis is in compliance with the journal's copyright policy.

Title: Magnetomechanical Fetal Cardiac Imaging: Feasibility of a New Multimodal Technique

Short title: Magnetomechanical Fetal Cardiac Imaging

Authors: Tan Phan, MS[a], Janette F. Strasburger, MD[b], Gabriela Pazin Tardelli, Bs[a,c], Gretchen Eckstein, RN[b], Ronald T. Wakai, PhD[a]

[a]Department of Medical Physics, University of Wisconsin, Madison, Wisconsin, USA

[b]Department of Pediatrics, Division of Cardiology, Children's Hospital of Wisconsin-Milwaukee, Milwaukee, Wisconsin, USA

[c]Departamento de Física-FFCLRP, University of São Paulo, Ribeirão Preto, São Paulo, Brazil

Keywords: fetal magnetocardiography, fetus, electromechanical function, fetal arrhythmia, 21 optically-pumped magnetometer 22

This work was supported by the National Institutes of Health [grant numbers R01 23 HL63174 and R01 HL143485]

Postnatally, a comprehensive assessment of heart rhythm and function is obtained by recording ECG and echocardiography simultaneously. Every clinical-grade cardiac ultrasound scanner has an ECG input for this purpose. Prenatally, however, such assessments are not routinely possible. Fetal ECG suffers from modest signal quality, and fMCG is generally difficult to combine with other techniques because the sensors are highly susceptible to contamination from electronic interference.

In this study we demonstrate simultaneous fetal magnetocardiography-fetal echocardiography (fMCG-fEcho) using a modified version of an fMCG system we developed

recently (1). The system is based on a new type of magnetic sensor, known as an optically-pumped magnetometer (OPM), which is has been shown to perform as well as a superconducting quantum interference device (SQUID) sensor for many applications, including fMCG (2,3). A critical advantage of OPMs is their small size, which enables the replacement of large, expensive magnetically shielded rooms by person-sized magnetic shields. For this study, we modified a person-sized shield to incorporate access ports. This allowed a sonographer to reach inside and scan the patient while the OPM sensors remain shielded from the interference produced by the scanner electronics.

The study was approved by the University of Wisconsin-Madison Health Sciences IRB. Two methods of simultaneous fMCG-fEcho were demonstrated. The first method utilized signal post-processing of the fMCG to remove maternal and environmental interference, and the second method did not utilize post-processing and could be performed in real time. The post-processing method required the use of a timing signal connected to the ECG input of the scanner and the fMCG data acquisition system. The lag between the fMCG and fEcho was determined by time-aligning the timing signals. The segment of the fMCG corresponding to the fEcho tracing was then overlaid onto the image. The real-time method simply required connecting the fMCG signal directly to the ECG input through electronic filters to band-limit the signal and remove 60 Hz interference.

Figs. 1A-1C show fMCG-fEcho tracings taken from normal subjects, utilizing signal post-processing of the fMCG. Several advantages of post-processing are evident. The P-waves can sometimes be resolved following post-processing, whereas in the raw signal they are obscured. Also, multiple fMCG channels can be superimposed on the fEcho tracings. Figs. 1D-1E show data from fetuses with bradycardia. In lieu of cine, several consecutive frames are concatenated to allow display of many cycles. Fig. 1D is from a fetus with complete AV block at 23 weeks' gestation. Fig. 1E shows an example of a real-time fMCG-fEcho tracing taken from a fetus with long QT syndrome at 31-3/7 weeks' gestation. The maternal interference was low even without signal processing for reasons not completely understood.

Figure 1 A: Fetal magnetocardiography–fetal echocardiography (fMCG-fEcho) tracing from a normal fetus at 21-6/7 weeks' gestation obtained using a medium sweep speed. Two fMCG channels are shown in yellow. The light blue tracing above the pulsed Doppler tracing is a computer-generated random timing signal connected to the electrocardiographic (ECG) input of the scanner and the fMCG data acquisition system and is used to time align the fEcho and fMCG tracings. **B:** fMCG-fEcho tracing from a normal fetus at 28 weeks' gestation. Note that P waves (P) can be resolved. The fastest sweep

speed was used to maximize the temporal resolution. **C:** fMCG-fEcho tracing from a normal fetus at 29-2/7 weeks' gestation. **D:** fMCG-fEcho tracing from a fetus with complete atrioventricular block at 23 weeks' gestation. **E:** Real-time fMCG-fEcho tracing from a fetus with long QT syndrome at 31-3/7 weeks' gestation. Measurements of the isovolumic contraction time (IVCT) and isovolumic relaxation time (IVRT) are shown. A = A wave (flow due to atrial contraction); E = E wave (passive filling of ventricles); LV = left ventricular; QTc = corrected QT; V = V wave (ventricular outflow).

A:

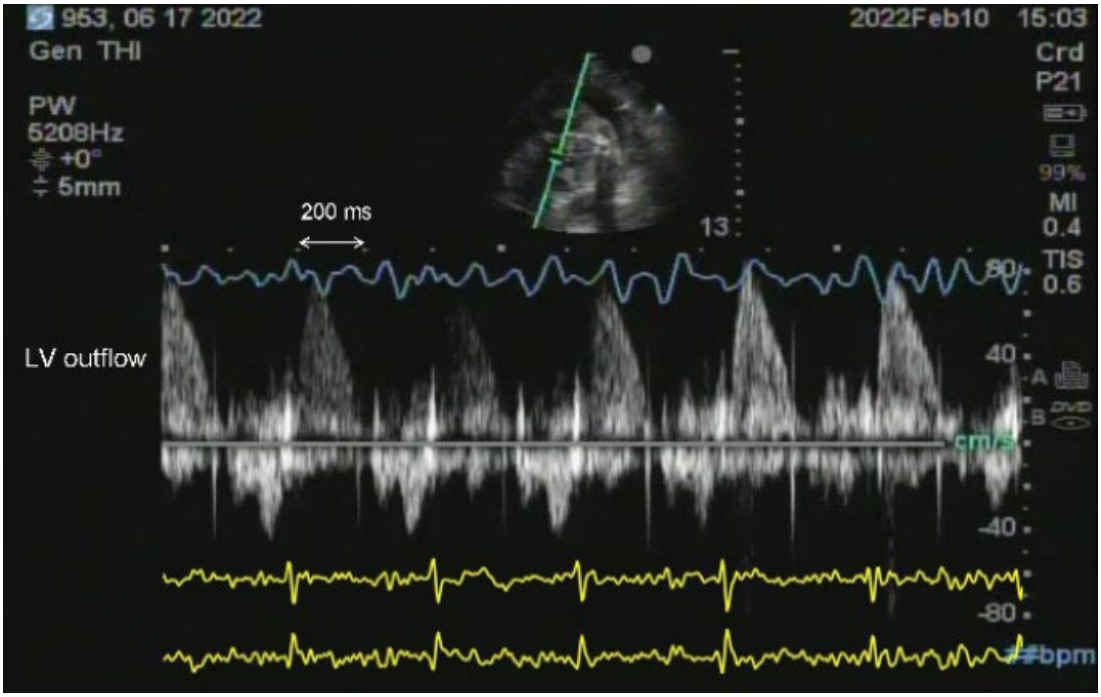

B:

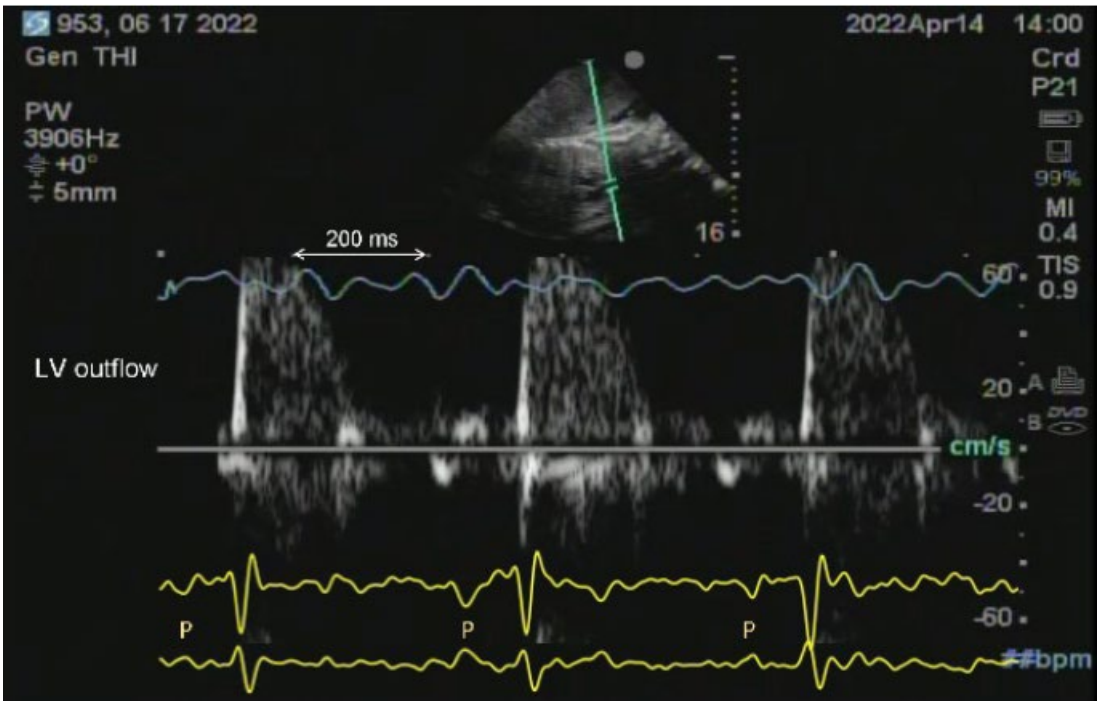

C:

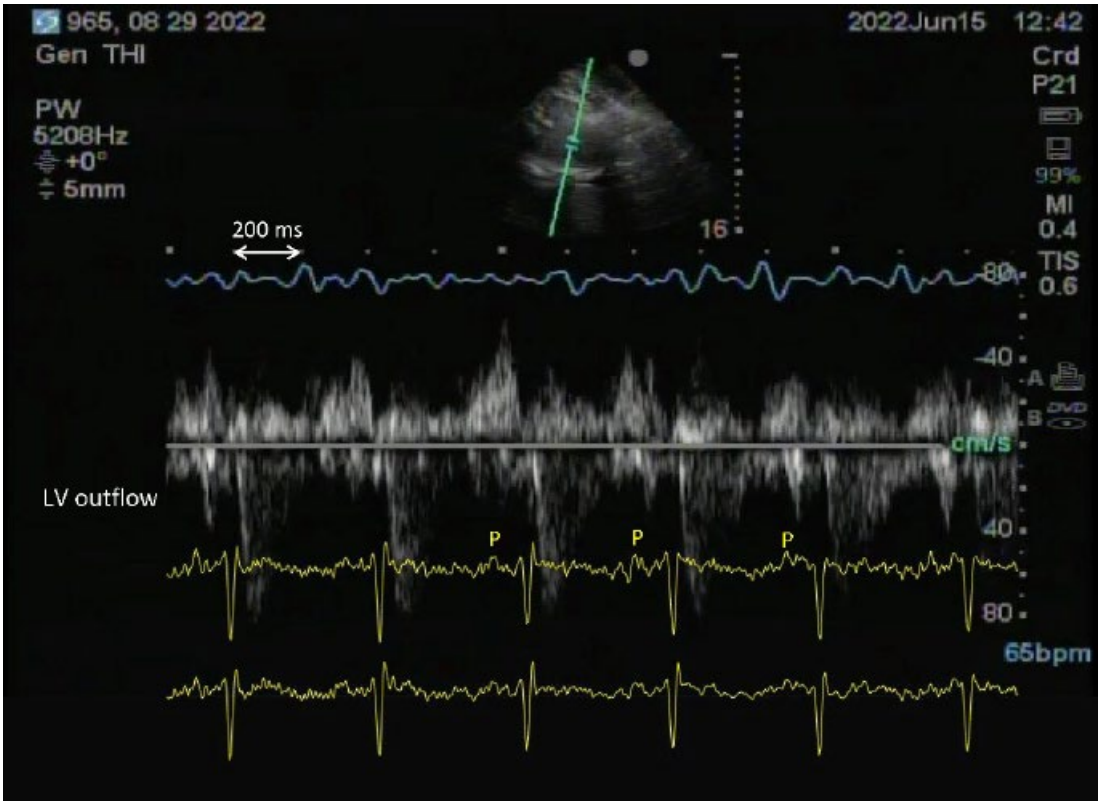

D:

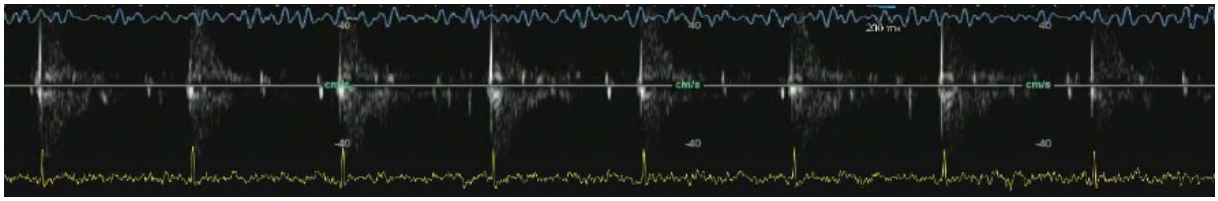

E:

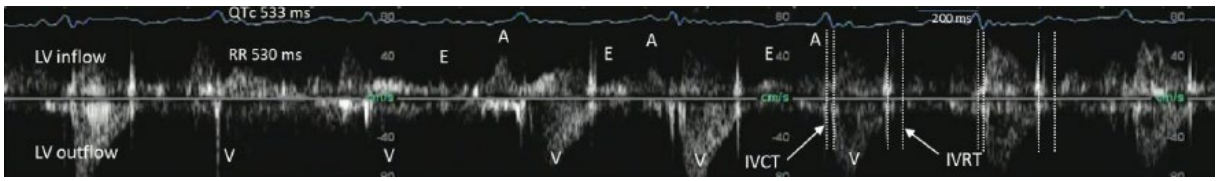

The results show that OPM technology can help overcome a major limitation of fMCG; namely, the difficulty of combining it with other modalities. The effectiveness of the methodology was evidenced by the first demonstration of real-time fMCG-fEcho. Simultaneous fMCG-fEcho allows direct comparison of the mechanical and magnetic rhythms. Potential applications include comparison of mechanical PR interval and fMCG PR interval in fetuses with incomplete AV block and isovolumic relaxation time and QTc interval in fetuses with long QT syndrome.

It also enables assessment of fetal electromechanical parameters, such as atrial activation time and pre-ejection period, and can aid the sonographer during scanning of complex, irregular rhythms.

The findings further demonstrate that fMCG—alone and in combination with fEcho—can overcome some of the current limitations of prenatal technology and extend several critical capabilities of postnatal cardiac monitoring to the fetus.

References:

1. Strand S, Lutter W, Strasburger JF, Shah V, Baffa O, Wakai RT. Low-Cost Fetal Magnetocardiography: A Comparison of Superconducting Quantum Interference Device and Optically Pumped Magnetometers. J Am Heart Assoc 2019;8:e013436.

2. Shah VK, Wakai RT. A compact, high performance atomic magnetometer for biomedical applications. Phys Med Biol;58:8153-61.

3. Batie M, Bitant S, Strasburger JF, Shah V, Alem O, Wakai RT. Detection of Fetal Arrhythmia Using Optically-Pumped Magnetometers. JACC Clin Electrophysiol 2018;4:284-287.